Analytical modelling of PCM supercooling including recalescence for complete and partial heating/cooling cycles

Maxime Thonon, Gilles Fraisse, Laurent Zalewski, Mickaël Pailha

Version of Record: https://www.sciencedirect.com/science/article/pii/S1359431121002064
Manuscript_186b809bb1b4739517e158c918221d70

Analytical modelling of PCM supercooling including recalescence for complete and partial heating/cooling cycles

Maxime Thonon[1,*], Gilles Fraisse[1], Laurent Zalewski[2], Mickael Pailha[1]

[1] Univ. Savoie Mont Blanc, CNRS, LOCIE, 73000 Chambéry, France

[2] Laboratoire de Génie Civil et géo-Environnement (LGCgE), Université d'Artois, ULR 4515, F-62400 Béthune, France

*Corresponding author: maxime.thonon@univ-smb.fr

Analytical modelling of PCM supercooling including recalescence for complete and partial heating/cooling cycles

Highlights :

- Analytical modelling of supercooling for complete and partial heating/cooling cycles
- The recalescence process is modelled considering the cooling rate and the enthalpy balance
- Experimental validation on a brick sample with heat flux and temperature measurements
- The model is validated experimentally for complete heating/cooling cycles and partial cooling cycles
- Modelling partial heating cycles require further investigation due to the influence of the crystalline structure on the phase change dynamic

Abstract:

Phase change material (PCM) experiencing supercooling and phase change hysteresis are widely reported in the literature. However, only few studies model analytically such PCM, and they mostly focus on either supercooling or phase change hysteresis, but rarely on both phenomena. Moreover, partial phase change cycles, with an incomplete melting or solidification, are rarely considered even if these processes occur frequently in latent heat thermal energy storage (LHTES) systems. The objective of this study is to model analytically the thermal behaviour of a PCM experiencing supercooling and phase change hysteresis, for complete and partial phase change cycles. The developed method, based on a heat source term, enables to model the recalescence process during the solidification. Currently rarely considered, the influence of the cooling rate on the supercooling degree and the recalescence process is evaluated with a phenomenological approach. For partial cycles, the different behavior between heating and cooling is modelled with the hysteresis model "curve scale" already validated in literature. The experimental validation is carried out on a PCM brick sample, monitoring both the heat flux and the PCM temperature, which enables to characterize a greater mass of PCM compared to direct scanning calorimeter (DSC) analysis. The selected PCM undergoing supercooling during solidification is PEG6000, a polymer suitable for domestic hot water (DHW) storage. Results show a good agreement between experimental and numerical results for complete heating and cooling cycles. The behavior laws used to model the solidification with the supercooling and recalescence processes are validated for the cooling rate range tested. The modelling is also satisfactory concerning the experiments on partial solidification for different temperature plateaus. However, the model fails to correctly represent the thermal behavior for a cooling process after a partial melting of the PCM. To conclude, the developed model enables to represent accurately the thermal behaviour of a PCM experiencing supercooling and phase change hysteresis for most of the phase change processes studied. Investigations on the thermal conditions influencing the crystalline structure and the effect on the phase change dynamic are suggested to improve supercooling modelling. The developed model needs to be validated for PCM having a higher supercooling degree, such as sugar alcohols or salt hydrates.

Keywords: Phase change material – Analytical modelling – Supercooling – Recalescence – Partial cycles – Hysteresis

Nomenclature

Variables

C_{eff}	$Effective\ heat\ capacity, J.kg^{-1}.K^{-1}$
Cp	$Specific\ heat\ capacity, J.kg^{-1}.K^{-1}$
f	$Liquid\ fraction$
H	$Enthalpy, J.kg^{-1}$
K	$Constants\ for\ behavior\ laws\ of\ recalescence$
L	$Latent\ heat, J.kg^{-1}$
m	$Mass, kg$
Q_{reca}	$Latent\ heat\ released\ during\ recalescence, J.kg^{-1}$
q_{reca}	$Power\ released\ during\ recalescence, W.kg^{-1}$
T	$Temperature, K$
t	$Time, s$

Greek letters

β	$Heating/Cooling\ rate, K.min^{-1}$
Δt_{reca}	$Recalescence\ duration, s$
λ	$Thermal\ conductivity, W.m^{-1}.K^{-1}$
ρ	$Density, kg.m^{-3}$
σ	$Coefficient: analytical\ modelling$
ε	$Coefficient: latent\ heat\ repartition$

Subscripts

H_x	$Heat\ exchanger$
L	$Liquid$
$Melt$	$Melting$
PC	$Phase\ change$
ref	$Reference$
S	$Solid$
SC	$Supercooling$
Sol	$Solidification$

Abbreviation

BPS	$Building\ performance\ simulation$
DHW	$Domestic\ hot\ water$
DSC	$Direct\ scanning\ calorimeter$
$LHTES$	$Latent\ \ heat\ thermal\ energy\ storage$
PCM	$Phase\ change\ material$
$PMMA$	$Poly(methyl\ methacrylate)$

1. Introduction

Latent heat thermal energy storage (LHTES) systems using phase change material (PCM) have been widely investigated and significantly developed this last decade through various applications [1], notably in the building sector [2–5] and for domestic hot water (DHW) storage [6]. The PCM is usually selected when its phase change temperature is suitable with the considered application [4,5], and when the energetic density and the thermal conductivity are as high as possible. Other parameters, such as supercooling during solidification, have to be taken into account to obtain a correct modelling and sizing of the LHTES. Supercooling is a phenomenon which might modify significantly the thermal behavior between melting and solidification; and therefore requires to be modelled correctly.

Supercooling is defined by a metastable state of the PCM, which remains liquid below the liquidus temperature of melting. During this stage, only sensible heat is exchanged with the environment. Some PCM, particularly sugar alcohols and salt hydrates, experience a significant supercooling when they are cooled [7]. The metastable state is usually broken by a heterogeneous nucleation when the first crystal appears on an impurity within the PCM or at the interface between the PCM and the container [8]. The temperature difference between the liquidus temperature of melting and the crystallization temperature is called the supercooling degree. Several studies highlighted that the faster the cooling rate, the higher the supercooling degree [8–11]. Nucleation triggering and crystals growth lead to a fast release of latent heat inside the material and a temperature increase of the PCM; this phenomenon is called the recalescence [12,13]. The temperature rise during the recalescence process depends on both the characteristic of the PCM and on the thermal exchange with the external environment. The remaining liquid fraction will be solidified after the end of the recalescence, when the temperature of the PCM sample is reduced further. During this step, the remaining content of latent heat of the PCM is completely released when the PCM reaches a fully solid state. Beaupere et al [14] prove experimentally that the degree of supercooling influences strongly the amount of heat released and the duration of the recalescence process.

The widespread experimental characterization of PCM by direct scanning calorimeter (DSC) is not possible for PCM experiencing supercooling. Indeed, the recalescence process cannot be observed as the temperature used to integrate the thermogram is the heat source temperature and not the PCM temperature, which is not monitored. Moreover, the temperature regulation of the DSC constrains the PCM to cool. Due to the very small size of the sample, the latent heat released, when the crystallization begins, is absorbed by the device and materialized by a heat flux peak. Therefore, there is no temperature rise of the PCM in DSC and the recalescence cannot be observed. Furthermore, the temperature where the metastable state is broken is influenced by the sample size [15–17] and the roughness of the container surface [18], extrapolating results from DSC, with a sample of only few milligrams, to real-scale applications, with several kilograms of PCM, is therefore not relevant. However, as explain later in this section, a hysteresis between the heating and cooling curves of DSC experiments might exist.

Analytical modelling of PCM without supercooling can be achieved by describing the thermodynamic state of the PCM with the evolution of the enthalpy $H(T)$, the effective heat capacity $C_{eff}(T)$ and the liquid fraction $f(T)$ in function of the temperature. As explained later, these three relations are equivalents and all of them can be used in the equation governing a phase change problem. The effective heat capacity $C_{eff}(T)$, defined as the derivative of the enthalpy $H(T)$, must not be confused with the apparent heat capacity, determined with DSC experiments by directly integrating the thermogram, which depends on the heating rate [19,20]. The DCS experiment (apparent heat capacity) would provide a result for the effective heat capacity when carried out with infinitely slow heating rate. However, the uncertainties increase for long DSC experiments because of the low heat flux measurements compared to the surrounding noises. For PCM with no supercooling

or a very low supercooling degree, as for paraffins and fatty acids [7], melting and solidification can be modelled analytically with a single expression ($H(T), C_{eff}(T)$ or $f(T)$) independent of the thermal solicitation of the PCM [21,22]. However, when the supercooling degree becomes significant, modelling supercooling requires to model complex phenomena, especially concerning the recalescence process, and is currently rarely considered for LHTES modelling.

The main difficulty of supercooling modelling is to obtain a correct representation of the thermal behavior of the PCM during its cooling, while ensuring a continuity of the enthalpy, temperature and liquid fraction within the PCM. Bony et Citherlet [23] propose a model based on an instantaneous isenthalpic transformation between the temperature of crystallization and the PCM enthalpic curve of melting. The model is only partially validated, the recalescence process is indeed numerically modelled but does not fit correctly with the experimental temperature. Instead of an isenthalpic transformation, Günther et al [24] suggest to use a heat source term to model the recalescence. With this method, heat is injected in each nodes of the numerical model when the node temperature falls below the nucleation temperature or when the liquid node is in direct contact with a solid neighbor node. A polynomial behavior law, dependent on the PCM temperature, is proposed to model the crystallisation kinetic within the PCM. Le Bot et Delauney [25] model the supercooling process of a metal by expressing the time evolution of the crystallized fraction, the reverse of the liquid fraction, with the product of a temperature function and a solidified-fraction function. A 2D model based on an enthalpic formulation is introduce by Uzan et al [26] and dissociates the PCM cooling process in four steps: liquid cooling while the PCM stays in a metastable state; kinetic nucleation to model the temperature increase during recalescence; regular solidification; and cooling of the solid phase. The crystallized fraction within the PCM is determined with a kinetic crystallization speed equation, which is dependent on the Gibbs activation energy. Jin et al [27] model supercooling with a heat source term which is function of a coefficient representing the latent heat release rate during the recalescence process. Recently, Davin et al [28] introduce a new formulation where the effective heat capacity is considered as negative during the recalescence process. Although thermodynamically impossible, using a negative effective heat capacity allows to model the temperature increase during the recalescence. A coefficient is integrated to consider the reaction kinetics by modifying the value of the negative effective heat capacity.

Whether or not the recalescence is considered into the numerical model, modelling a different thermal behavior between the heating and cooling processes of a PCM requires to define a hysteresis with two distinct curves of $H(T)$, $C_{eff}(T)$ and $f(T)$. This hysteresis phenomenon between the heating curve (red curve Figure 1) and the cooling curve (blue curve Figure 1) is observed experimentally either by DSC methods or T-history methods [29]. As shown by Mazzeo et al [30], on a recent comparative study on commercial building performance simulation (BPS) softwares, considering a phase change hysteresis enables a better modelling of the LHTES. Using a hysteresis between the heating and cooling curves raises the issue of partial phase change cycles from a numerical perspective. As for modelling the recalescence process, it is necessary to ensure a continuity of the temperature, the enthalpy and the liquid fraction within the PCM during partial cycles.

Liu et al [31] and Klimeš et al [32] provide a comprehensive summary on recent experimental measurements and numerical modelling of hysteresis for PCM. Thanks to hysteresis modelling, Fateh et al [33] reach a correct representation of the temperature and heat exchanges, for a PCM incorporated into an insulation layer, for complete melting and solidification. Still working on complete phase change, Kumarasamy et al [34] obtain satisfactory results, thanks to the hysteresis modelling of an encapsulated PCM, in comparison with results from DSC experiments. Goia et al [35] also model accurately the temperature of a PCM incorporated into a wall for complete melting and solidification. However, modelling of partial phase change cycles, with the hysteresis model “curve switch” (orange curves Figure 1), which switch from one curve to the other with a constant liquid fraction, shows a significant error and is not validated. Delcroix et al [36] study the performances of hysteresis model “curve switch” and “curve track” (green curves Figure 1), where the PCM follows in the opposite direction the curve used at the time of the temperature inversion. Results show that “curve track” model is neither relevant for partial melting nor for partial solidification. The hysteresis model “curve switch” represents accurately partial solidification but does not model correctly partial melting. An optimized solution, reducing the error between numerical and experimental results, is proposed by the authors to model partial melting by adding an intermediate enthalpy curve between the heating and cooling curves. Barz et Sommer [37] present a comparative study of four hysteresis models. Two models, “curve track” and “curve scale”, are found to be static and independent from the thermal load. The hysteresis model “curve scale” (purple curves Figure 1) is theoretically formulated by Ivshin et Pence [38]. It consists of following the shape of the second curve, from the point where the heating or cooling process is interrupted, with a scale factor, dependent of the interruption point of heating or cooling, to guarantee a continuity of the liquid fraction. The two other models, “melting/solidification kinetic” and “solidification kinetic”, are dynamics and depends on the thermal load. The authors conclude that the static hysteresis model “curve scale” presents the best performances and recommend it for partial phase change modelling. A second comparative study made by Barz et al [39] on hysteresis models “curve track”, “curve switch” and “curve scale” reaches the same conclusions. Finally, Jin et al [27] obtain a correct representation of partial phase change for an inorganic PCM, but only few details are provided by the authors on the hysteresis model used.

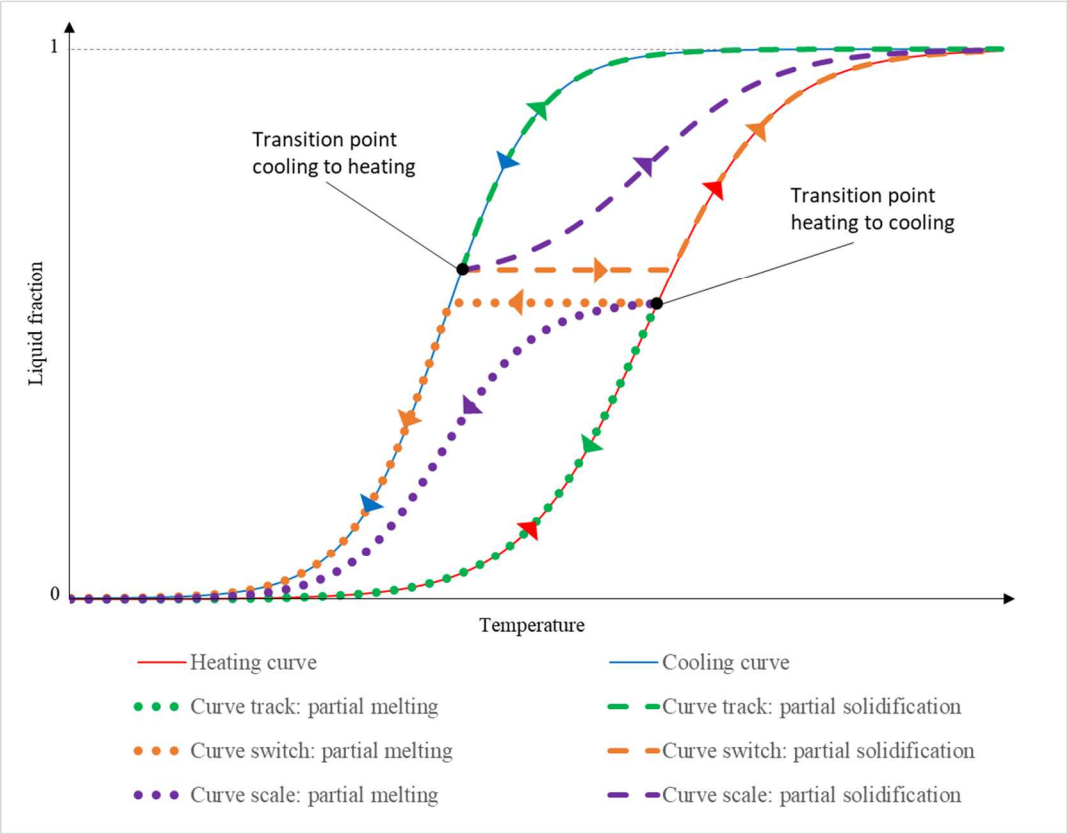

Figure 1: Schematic diagram of hysteresis model « curve track », « curve switch » and « curve scale »

Table 1 summarizes the methods and assumptions of the different studies from the literature detailed in this section. The first column, "Modelling recalescence (cooling)", specifies if the authors model numerically the recalescence process and by which method. The second column, "Modelling supercooling with hysteresis (Heating/Cooling)", shows authors using two distinct curves to model the PCM thermal behavior during heating and cooling cycles. The two sub-columns dissociate when the modelling consider complete or partial phase change cycles. Finally, the last column details which reference, temperature or heat flux, is considered to validate the numerical model with the experimental results. Table 1 shows that most studies focus only on supercooling modelling or phase change hysteresis modelling, but rarely on both phenomena. Moreover, most of the time, partial phase change cycles are not studied even if these processes occur frequently in LHTES systems. Finally, the experimental validation is rarely conducted both for temperature and heat flux.

Table 1: Synthesis of recalescence model and hysteresis model proposed in the literature

	Modelling recalescence (Cooling)	**Modelling supercooling with hysteresis (Heating/Cooling)**		**Validation**	
		Complete phase change	*Partial phase change*	*Temperature*	*Heat flux*
Bony et Citherlet [23]	Isenthalpic	No	No	Partly	No
Günther et al. [24]	Heat source	No	No	Yes	No
Le Bot et Delaunay [25]	Heat source	No	No	Yes	No
Delcroix et al. [36]	No	Yes	No	Yes	No
Uzan et al. [26]	Kinetic laws	No	No	Yes	No
Fateh et al [33]	No	Yes	No	Yes	Yes
Kumarasamy et al. [34]	No	Yes	No	No	Yes
Barz et Sommer. [37]	No	Yes	Yes	Yes	No
Goia et al. [35]	No	Yes	No	Yes	No
Barz et al. [39]	No	Yes	Yes	Yes	No
Davin et al [28]	Negative C_{eff}	No	No	Yes	No

Jin et al [27] *(few details)*	Heat source	Yes	Yes	Yes	Yes

The objective of this article is to achieve an analytical modelling of a PCM undergoing supercooling during its cooling. Compare to the existing state of the art presented in Table 1, the developed model considers both supercooling and phase change hysteresis for complete and partial phase change cycles. To our best knowledge, only the work of Jin et al [27] includes an analytical modelling of the recalescence and of the hysteresis for partial cycles. However, the analytical formulation chosen by Jin et al [27] is basic, with a constant effective heat capacity to describe the thermodynamic state of the PCM. The authors do not provide enough elements to evaluate the hysteresis model for incomplete phase change, but results show a good agreement with the experiments.

The propose method to model supercooling allows to consider the influence of boundary conditions on both the temperature where the metastable state is broken and the recalescence process, which is currently rarely taken into account. Moreover, the developed methodology enables to determine, from an enthalpy energy balance, the amount of latent heat released during the recalescence process. The hysteresis between cooling and heating is taken into account by the model for complete and partial phase change cycles thanks to phenomenological formulations from the literature. Furthermore, the results from our numerical model are compared to those obtain experimentally with a brick filled with PCM which, contrary to results from DSC experiments on small samples, enables to get closer to the real behavior of a LHTES. The model is evaluated considering both the experimental temperature inside the PCM and the heat flux exchanged between the brick outer surface and the heat exchangers, which apply a controlled temperature on the surface. In most cases, existing studies validate the numerical model of supercooling or hysteresis only on temperature which is a local measurement. The heat flux, a global measurement, between the sample and the surrounding are rarely considered. However, as explain later, considering only temperature or heat flux might lead to a misinterpretation of the PCM thermal behavior by omitting some phenomena (see part 4.2).

In this study, we chose polyethylene glycol 6000 (PEG6000) as PCM experiencing supercooling while being cooled. It is a polymer widely used in the medical and cosmetic sectors. As other polymers, it might be used for constructing LHTES units thanks to good thermal performances and a lower price compared to fatty acids and paraffins [40]. PEG6000 is particularly adapted for DHW storage due to its phase change temperature close to $60°C$ [41]. Crystallization of polymers involves complex phenomena and has been extensively studied last decades [42]. Microscopic observations show the influence of the cooling rate on the crystalline structure of the solid phase [43] and the first crystals to melt are the last ones to have been crystalized [44]. Concerning PEG6000, Vehreyen et al [45] highlighted that the crystalline structure of the solid phase, which depends on the cooling conditions, affects the melting dynamic of the PCM.

2. Description of the model

2.1. Phase change modelling without supercooling

Analytical modelling of PCM with no supercooling can be described by a unique equation independent of the heating and cooling rate. The accuracy of the modelling depends on the equation selected and a wide variety of analytical formulations exist in the literature [21]. They describe the thermodynamic state of the PCM either according to the evolution of the liquid fraction $f(T)$, mostly with a linear variation on the phase change temperature range [46–50], the evolution of the effective heat capacity $C_{eff}(T)$, often with a gaussian function [26,28,39,51–54] or a sigmoid function [55], or the evolution of the enthalpy $H(T)$, from a binary solution for example [56]. The equation governing a phase change problem can be defined by equation (1) if $H(T)$ is known, by equation (2) if $C_{eff}(T)$ is known, or by equation (3) if $f(T)$ is known.

$$\rho * \frac{\partial H(T)}{\partial t} = \lambda * \nabla^2 T \qquad (1)$$

$$\frac{\partial T}{\partial t} = \frac{\lambda}{\rho * C_{eff}(T)} * \nabla^2 T \qquad (2)$$

$$\frac{\partial T}{\partial t} = \frac{\lambda}{\rho * \left(Cp_S + (Cp_L - Cp_S) * f(T) + L * \frac{df(T)}{dT} \right)} * \nabla^2 T \qquad (3)$$

The comparative study on analytical modelling of Thonon et al [21] showed the best accuracy for the equation describing the liquid fraction with the derivative of an asymmetric gaussian function. This equation is therefore selected for this study and is presented according to $f(T)$ with equation (4), according to $C_{eff}(T)$ with equation (7), and according to $H(T)$ with equation (8). Temperatures T_S and T_L refer to the highest temperature where the PCM is fully solid and the lowest temperature where the PCM is fully liquid, respectively. Coefficients σ_S from equation (5) and σ_L from equation (6) enable to guarantee a liquid fraction close to 0 at T_S and close to 1 at T_L. The maximum of the effective heat capacity is reached at T_{PC}, which corresponds to the highest slope on the enthalpy and liquid fraction curves. Figure 2 illustrates the kind of curve

which could be obtained, for a PCM with a single heat flux peak, with the analytical model selected in this study according to $f(T)$, $C_{eff}(T)$ and $H(T)$.

$$f = \begin{cases} \frac{\sigma_S}{\sigma_S + \sigma_L} * \left[er\,f\left(\frac{T - T_{PC}}{\sigma_S}\right) + 1 \right] & T \leq T_{PC} \\ \frac{1}{\sigma_S + \sigma_L} * \left[\sigma_L * er\,f\left(\frac{T - T_{PC}}{\sigma_L}\right) + \sigma_s \right] & T > T_{PC} \end{cases} \quad (4)$$

$$\sigma_S = \frac{\sqrt{2}}{4} * (T_{PC} - T_S) \quad (5) \qquad \sigma_L = \frac{\sqrt{2}}{4} * (T_L - T_{PC}) \quad (6)$$

$$C_{eff} = \begin{cases} Cp_S + (Cp_L - Cp_S) * f_{erf}(T) + \frac{2 * L}{(\sigma_S + \sigma_L).\pi^{0.5}} * exp\left(-\left(\frac{T - T_{PC}}{\sigma_S}\right)^2\right) & T \leq T_{PC} \\ Cp_S + (Cp_L - Cp_S) * f_{erf}(T) + \frac{2 * L}{(\sigma_S + \sigma_L) * \pi^{0.5}} * exp\left(-\left(\frac{T - T_{PC}}{\sigma_L}\right)^2\right) & T > T_{PC} \end{cases} \quad (7)$$

$$H = Cp_S * \left(T - T_{ref}\right) + (Cp_L - Cp_S) * \int_{T_{ref}}^{T} f_{erf}(T)dT + L * f_{erf}(T) \quad (8)$$

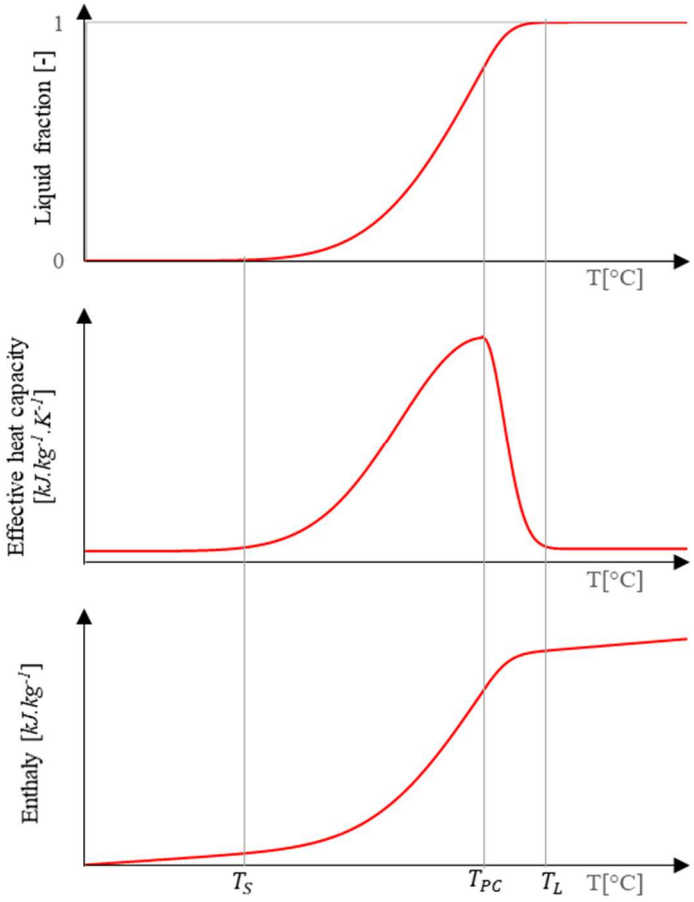

Figure 2: Example of the evolution of the liquid fraction, effective heat capacity and enthalpy as a function of temperature.

Sometimes, several heat flux peaks might be observed during the heating or cooling processes of a PCM if it is not entirely pure or composed by different crystalline structures within the solid phase *[57–60]*. An accurate modelling of these PCM requires to dissociate the different structures/materials into distinct phases as detailed by Thonon et al *[21]*. If the PCM is composed by two materials/structures A and B, equation (4) and equation (7) are then modified into equation (9) and equation (10) , respectively. As the mass fraction of materials/structures A and B is unknown, it is necessary to assume that the two materials/structures have an equivalent latent heat, e.g. $L_A \approx L_B$, to define the mass fraction of each materials. The contribution to the total latent heat of the PCM by materials/structures A and B is then represented in equations and by L_1 and L_2, respectively. In these conditions, the ratio between L_1, the share of the total latent heat of the PCM associated to material/structure A, and $L_1 + L_2$, the total latent heat of the PCM, enables to define de mass fraction of material/structure A.

$$f_{Tot}(T) = f_A(T) * \frac{L_1}{L_1 + L_2} + f_B(T) * \frac{L_2}{L_1 + L_2} \quad (9)$$

$$C_{eff}(T) = Cp_S + (Cp_L - Cp_S) * f_{Tot}(T) + L_1 * \frac{df_A(T)}{dT} + L_2 * \frac{df_B(T)}{dT} \quad (10)$$

2.2. *Supercooling modelling during solidification*

Modelling supercooling during the PCM cooling cycle is achieved by considering three phenomenological steps described below and presented on Figure 3:

- Metastable state: The PCM remains liquid in a metastable state below the highest temperature where a solid phase exists during the heating cycle (Temperature T_L on Figure 2). During this stage, only sensible heat is exchanged.
- Recalescence: Once the PCM reaches temperature $T_{reca\ start}$, the metastable state is broken and the crystallization starts inside the PCM. The beginning of the crystallization and the crystals growth are associated to a sharp release of latent heat inside the PCM. The latent heat release leads to an increase of the PCM temperature, and therefore to a partial transfer of this heat to the external environment. At the end of the recalescence process, the temperature is equal to $T_{reca\ end}$ and a part of the PCM is solidified.
- Regular solidification: When the recalescence process is over, the remaining quantity of liquid PCM defines the amount of latent heat that can be extracted before reaching a fully solid state

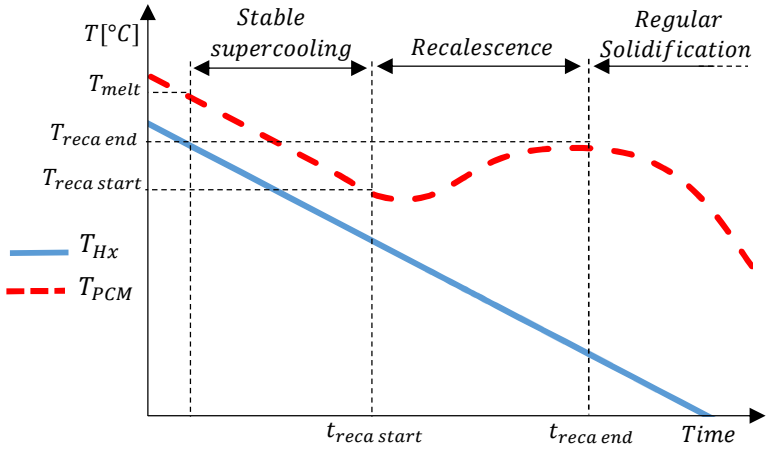

Figure 3:Phenomenological stages observed during the solidification of a PCM with supercooling

The methodology to model supercooling introduces in this article is presented with Figure 4 and developed in detail below. On Figure 4, to facilitate understanding of the model and to avoid unnecessary complicated explanations and figures , solid and liquid specific capacities are considered equal, the PCM consists of a single material/structure (equations (4), (7) and (8)), and the analytical functions used to model regulars melting and solidification of the PCM have the same shape. These simplifying assumptions are only used in this section to explain the model and are not considered in the developed model.

At the stable supercooled state, the PCM is fully liquid until the temperature falls below temperature $T_{reca\ start}$, where the metastable state is broken and the recalescence begins. The degree of supercooling ΔT_{SC} defines the temperature gap between $T_{L\ melt}$ (point A Figure 4), the highest temperature where a solid phase exists inside the PCM during the heating cycle, and temperature $T_{reca\ start}$ (point B Figure 4). Several studies show a dependency of the temperature $T_{reca\ start}$ with the cooling rate β of the PCM [8,10,11,37]. In this study, equation (11) is proposed to evaluate temperature $T_{reca\ start}$ with two constants K_1 and K_2 specific to the considered PCM. The power law formulation of equation (11) enables to reach toward a plateau, where an increase of the cooling rate β will almost not impact anymore $T_{reca\ start}$, as physically the nucleation probability is close to 100%.

$$T_{reca\ start} = \begin{cases} K_1 * \beta^{-K_2} & T < T_{L\ melt} \\ T_{L\ melt} & T > T_{L\ melt} \end{cases} \quad (11)$$

When temperature $T_{reca\ start}$ is reached, the first crystal appears and the recalescence process starts with the crystals growth [61]. The amount of latent heat Q_{reca} releases during the recalescence is obtain by reasoning theoretically on a PCM with adiabatic boundary conditions. In these conditions, theoretically, the PCM undergoes an isenthalpic transformation from temperature $T_{reca\ start}$ (point B Figure 4) to $T_{reca\ end\ adiab}$ (point C Figure 4), the temperature at equivalent enthalpy on the heating curve [62]. The enthalpy $H_{reca\ start}$, at the beginning of the recalescence, is determined with equation (12) and the

temperature $T_{reca\ end\ adiab}$ is obtained numerically by solving equation (13) with the PCM analytical equation of melting (equation (8)).

$$H_{reca\ start} = H_{SC}(T_{reca\ start}) = H_{melt}(T_{L\ melt}) - Cp_L * (T_{L\ melt} - T_{reca\ start}) \quad (12)$$

$$H_{reca\ start} = H_{melt}(T_{reca\ end\ adiab}) \quad (13)$$

In this theoretical configuration, the enthalpy gain, associated to the temperature increase, is balanced by a decrease of the liquid fraction in order to ensure an isenthalpic transformation. Between the start and the end of the recalescence, the liquid fraction evolves from $f_{reca\ start} = 1$ (point B in the middle section of Figure 4) to $f_{reca\ end} = f_{melt}(T_{reca\ end\ adiab})$ (point C in the middle section of Figure 4). It is then possible to obtain the latent heat released during the recalescence process with equation (14). The effective heat capacity is assumed constant and equal to the liquid value Cp_L during the recalescence, from point B to point C^*. At the end of the recalescence, where only a part of the PCM is crystalized, the transition to the regular solidification process is modelled by an effective heat capacity jump from point C^* to point C on Figure 4.

$$Q_{reca} = L_{melt} * (1 - f_{reca\ end}) = H_{SC}(T_{reca\ end\ adiab}) - H_{melt}(T_{reca\ end\ adiab}) \quad (14)$$

However, an accurate modelling of supercooling requires to use the real boundary conditions of the system, and they cannot be considered adiabatic as the heat exchangers removed heat from the PCM during the cooling cycle. This means that a part of the latent heat Q_{reca} releases during the recalescence is removed from the PCM to the external environment. The real temperature of the PCM $T_{reca\ end}$ at the end of the recalescence is therefore lower than the theorical temperature $T_{reca\ end\ adiab}$. However, the liquid fraction inside the PCM is only dependent on the quantity of latent heat Q_{reca} released, and remains equal to $f_{melt}(T_{reca\ end\ adiab})$ at the end of the recalescence, regardless of the value of $T_{reca\ end}$.

A theoretical isothermal recalescence can also be defined. If all the latent heat released during the recalescence is removed directly to the external environment, this would lead to an isothermal transformation without temperature increase of the PCM (transition from point B to point D Figure 4). At the end of the recalescence, a regular solidification occurs to completely solidify the PCM.

With real boundary conditions, the temperature increase of the PCM, during the recalescence, follows an intermediate path between the theoretical adiabatic and isothermal recalescences, as the aim of a LHTES is to extract the stored heat with an non-ideal heat exchanger. A part of the energy is extracted and the other part of the latent heat is released inside the PCM, leading to a characteristic temperature rise. Temperature $T_{reca\ end\ real}$ at the end of the recalescence is plotted by point E on the CD segment Figure 4. Transition from point B to E during the recalescence is represented with a straight line on Figure 4, but this is usually not the case as the shape depends on the heat removal between the PCM and the external environment. As for an adiabatic recalescence, the evolution of the effective heat capacity is considered equal to the liquid specific capacity of the PCM during the recalescence between point B and E^*. The effective heat capacity jump between points E^* and E at the end of the recalescence enables to model a slow cooling, with a temperature plateau, during the regular solidification of the PCM.

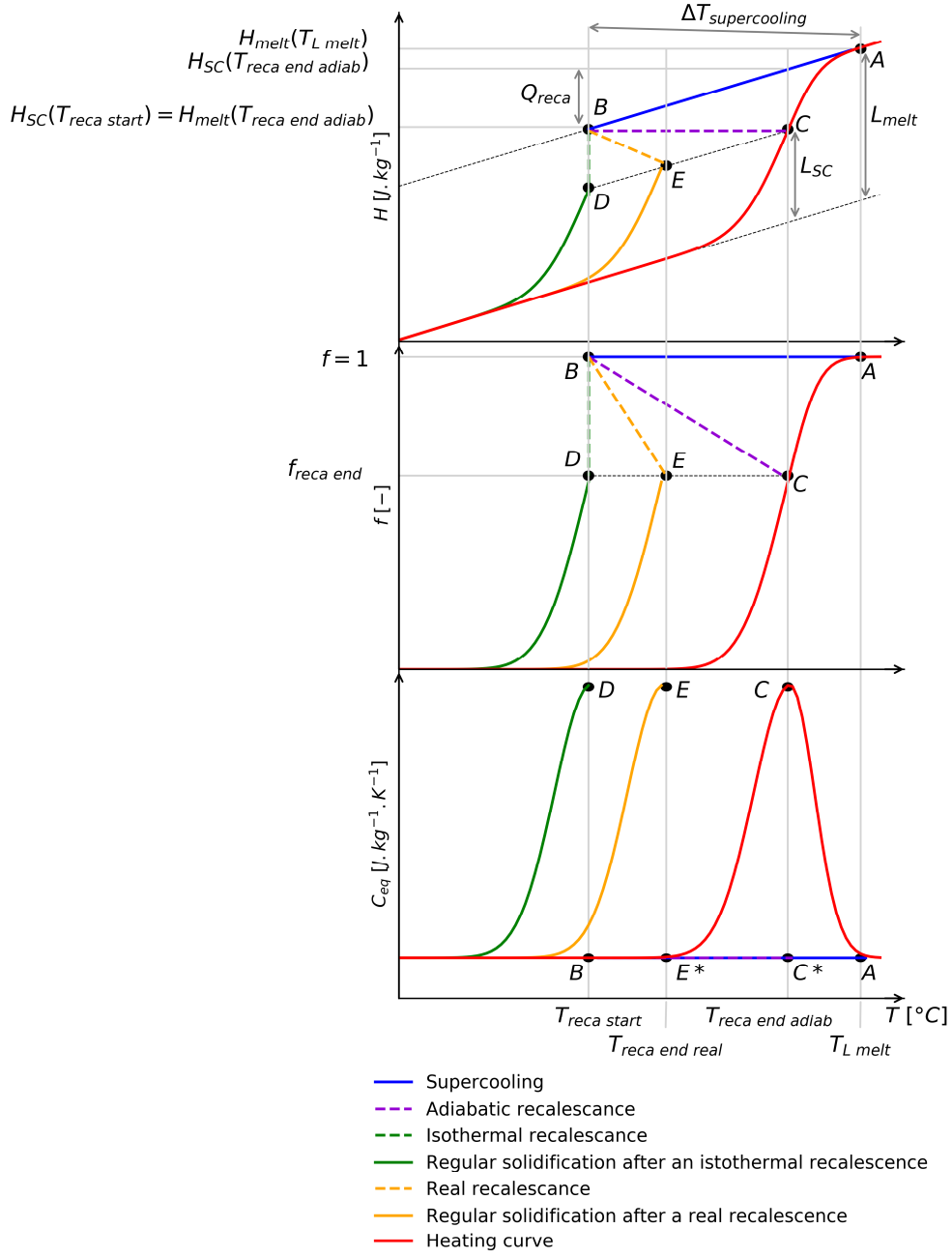

Figure 4: Evolution of the enthalpy (top), liquid fraction (middle) and effective heat capacity (bottom) for the supercooling model proposed in this work.

Besides influencing $T_{reca\ start}$, the cooling rate of the PCM impacts the kinetic of crystallization of the solid phase, and thus the duration of the recalescence Δt_{reca} [63–65]. In this study, to simplify the modelling, the physical laws describing the kinetic of crystallization are not incorporated into the model but estimated with behavior laws. The recalescence is considered to begin at time $t_{reca\ start}$ in the entire PCM, and the duration of the recalescence Δt_{reca} is obtained with equation (15). The power law enables to limit the crystallization speed for fast cooling rates, constants K_3 and K_4 being specific to the studied PCM.

$$\Delta t_{reca} = K_3 * \beta^{-K_4} \qquad (15)$$

Now that $T_{reca\ start}$, Q_{reca}, $f_{reca\ end}$ and Δt_{reca} have been determined, the last unknown parameter to model the recalescence is the heat release profile $q_{reca}(t)$. This profile is defined by equation (16) and ensures that the entirety of Q_{reca} is released during Δt_{reca} as shown by equation (17). The second order polynomial equation from Equation (16) enables to represent accurately the temperature rise, at the beginning of the recalescence, with a sharp increase of the latent heat released inside the PCM. At the end of the recalescence, the quasi temperature plateau is also correctly estimated with Equation (16) thanks to a slight increase of the latent heat released.

$$q_{reca}(t) = \frac{-3 * Q_{reca}}{2 * \Delta t_{reca}^3} * (t - t_{reca\ start})^2 + \frac{3 * Q_{reca}}{\Delta t_{reca}^2} * (t - t_{reca\ start}) \quad (16)$$

$$\int_{t_{reca\ start}}^{t_{reca\ end}} q_{reca}(t) = Q_{reca} \quad (17)$$

At the end of the recalescence, the latent heat L_{SC} still inside the PCM is obtained with equation (18) by removing the latent heat Q_{reca}, released during the recalescence, to the melting latent heat L_{melt}. The PCM will be fully liquid once all the latent heat L_{SC} inside the material will have been released during the solidification. A regular solidification is used to model the end of the solidification. This regular solidification is described by an analytical equation equivalent to the one used for a phase change without supercooling (equations (4),(7) and (8)), but with a set of parameters ($T_{S\,SC}, T_{PC\,SC}, T_{L\,SC}$) specific to the regular solidification, which is different than the one used for melting modelling. At the beginning of the regular solidification, the mean temperature of the PCM is equal to $T_{reca\ end}$, and the mean liquid fraction of the PCM $f_{SC}(T_{reca\ end})$ is equal to $f_{reca\ end}$ (equation (19)). However, as the boundary conditions are not adiabatic, the temperature is not homogeneous inside the PCM. The main difficulty consists to obtain a unique equation to describe the thermodynamic state of the PCM, while satisfying the equality of equation (19). This is achieved by imposing $T_{L\,SC} = T_{PC\,SC} = T_{reca\ end} + K_5$, with K_5 a constant specific to the studied PCM. Then, temperature $T_{S\,SC}$ is the last unknown to identify to obtain the analytical equations describing the regular solidification with equations (4), (7) and (8). Given that only one temperature allows to satisfy equation (19), if temperatures $T_{L\,SC}$ and $T_{PC\,SC}$ are fixed as explained above, $T_{S\,SC}$ is solved numerically.

$$L_{SC} = L_{melt} - Q_{reca} \quad (18)$$

$$f_{SC}(T_{reca\ end}) = f_{reca\ end} \quad (19)$$

The methodology introduces above, to model analytically supercooling and the recalescence process, has the benefit to consider the boundary conditions, but also the impact of the cooling rate on the recalescence process, which is rarely achieved in most of the existing models. However, the analytical equation describing the regular solidification (equations (4),(7) and (8) in the simplified model detail in this section) remains unknown before the end of the recalescence as the boundary conditions influence the recalescence.

2.3. Hysteresis modelling for partial phase change

As mentioned in the introduction, melting modelling (section 2.1) and supercooling modelling (section 2.2) of the PCM lead to a phase change hysteresis between the two curves, either for $f(T), C_{eff}(T)$ or $H(T)$. The main issue is to ensure, for partial cycles of heating and cooling, a continuity of the temperature, the liquid fraction and the enthalpy of the PCM.

Partial solidification, when the PCM is reheated before reaching a fully solid phase, is modelled with the phenomenological hysteresis model "curve scale" introduced by Ivshin et Pence [38] and validated by Barz et al [39]. The comparative study on hysteresis models performed by Barz et al [39] concludes by recommending the "curve scale" model which presents better performances than "curve track" and "curve switch" models. Temperature T_0 and liquid fraction $f(T_0)$ of the "curve scale" model defined by equation (20) refer to the temperature and liquid fraction of the PCM where the cooling cycle is interrupted. With this hysteresis model, the liquid fraction follows, with a scaling factor, the liquid fraction of the heating curve f_{melt}, which it the reference. The orange dashed curve of Figure 5 illustrates the "curve scale" hysteresis model for a reheating cycle after a partial solidification.

$$f(T) = 1 - \frac{1 - f(T_0)}{1 - f_{melt}(T_0)} * \left(1 - f_{melt}(T)\right) \quad (20)$$

Modelling partial melting is more complex for multiple reasons. First, it has been shown that PCM undergoing a partial melting cannot reach a metastable state during their cooling, as there is still a solid phase inside the PCM to initiate the crystallization [14]. In this study, we suppose that a liquid fraction higher than 95% is necessary to maintain a metastable state during the cooling cycle. Below this threshold, the PCM does not show supercooling while being cooled. This assumption is valid regarding the low thermal gradient within the PCM sample and the narrow width of the brick used for the experiments (section 3.1). However, for large PCM volume and under specific thermal boundary conditions, a solid phase and a supercooled phase might coexist and a 95% threshold may not be relevant. Even if the PCM is not fully liquid, it is necessary to consider a hysteresis from the heating curve during the solidification. Indeed, the "curve track" hysteresis model, relying on following the heating curve on the opposite direction, does not reproduce correctly the thermal behavior of a partially melted PCM being cooled [36,39]. Modelling numerically the hysteresis requires to define a reference curve for cooling when the PCM does not show supercooling. It is not possible to use the cooling curve defining the regular solidification after the recalescence for fully liquid PCM. Indeed, this curve is unknown before the end of the recalescence (section 2.2) and will therefore be unknown for a partial melting with no supercooling during the solidification. It is then necessary to implement a reference curve, for a solidification after a partial melting, to the hysteresis model. This reference curve is described according to $f(T)$ by equation (4) with a set of parameters ($T_{S\,sol}, T_{PC\,sol}, T_{L\,sol}$) specific to cooling after a partial melting, and is plotted in green on Figure 5. As for partial solidification, the hysteresis model "curve scale" is also selected for partial melting. It is defined by equation (21) where T_0 and $f(T_0)$ refer to the transition point where the heating

cycle is interrupted. Figure 5 illustrates with the dashed green curve the “curve scale” hysteresis model for a partial melting followed by a cooling cycle.

$$f(T) = \frac{f(T_0)}{f_{sol}(T_0)} * f_{sol}(T) \qquad (21)$$

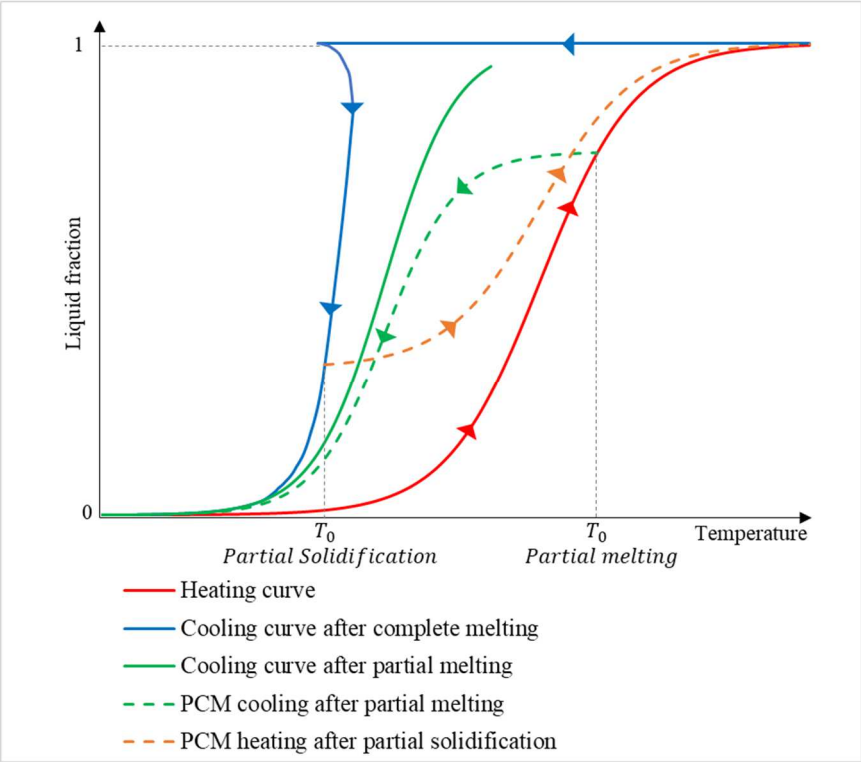

Figure 5: «Curve scale» hysteresis model for partial melting and partial solidification

3. Experimental apparatus and identification of PCM properties

3.1. Experimental apparatus

Presented by Figure 6, the experimental apparatus is a fluxmeter bench, similar to the one used by Younsi et al [66], Joulin et al [67,68] and Tittelein et al [69]. The set-up enables to apply heat loads to a poly(methyl methacrylate) (PMMA) brick filled with PCM. The description of the experimental apparatus, the measurement principle and the accuracy of the instrumentation (tangentiel gradient heat fluxmeters and thermocouples) have been described in a previous work (Thonon et al [21]). The temperature on the two large faces of the PMMA brick is imposed by the two heat exchangers, which are controlled by thermo-regulated baths. Fluxmeters, with an integrated thermocouple, are located on each face of the brick. The fluxmeters located on the large two faces of the brick monitor the heat transfers between the sample and the heat exchangers. A thermocouple is also immersed in the PCM, at the middle of the brick, to monitor the PCM temperature. The lateral sides of the brick are enclosed with an insulation layer to avoid thermal losses. The identical thermal load on each face, the limited lateral losses (verified with the lateral fluxmeters) and the narrow width of the sample, enable to assume a 1D heat problem and to avoid natural convection inside the PCM.

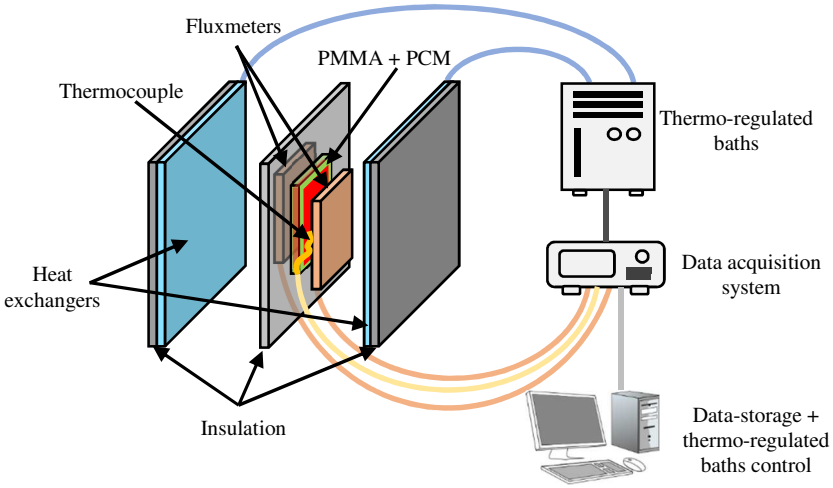

Figure 6: Experimental apparatus

3.2. *Experimental protocol*

A mass of $285g$ of liquid PEG6000 is incorporated inside the PMMA brick. For the whole set of experiments, the same temperature is applied on each face of the brick by the heat exchangers. The experiments are caried out with different heating and cooling rates β for complete and partial phase change cycles. The two first sets of experiments focus on complete melting and solidification cycles between $20°C$ and $70°C$ with a duration of $3h$, $4h$, $5h$ and $18h$. The two next sets of experiments consists of partial cycles, for a ramp $\beta = 0.2\ K.min^{-1}$ and a plateau of $3h$ before returning to the initial temperature, with temperature plateaus of 55-57-62-67$°C$ for partial melting cycles and temperature plateaus of 55-50-45-40$°C$ for partial solidification cycles. Finally, still with a ramp $\beta = 0.2\ K.min^{-1}$, a series of partial cycles is carried out with an initial temperature of $70°C$, followed by temperature plateaus of 55-65-50-60-45-55$°C$, before ending to the final temperature at $20°C$. Table 2 summarizes all the experiments performed in this study by detailing the initial and final temperatures, the possible temperature plateaus, the heating/cooling rate applied, and the duration of the experiment.

Table 2: list of experiments conducted

	T_{start} $[°C]$	$T_{plateau}$ $[°C]$	T_{end} $[°C]$	β $[K.min^{-1}]$	$Duration$ $[h]$
Complete melting	20	–	70	0.278	3
Complete melting	20	–	70	0.208	4
Complete melting	20	–	70	0.167	5
Complete melting	20	–	70	0.046	18
Complete solidification	70	–	20	−0.278	3
Complete solidification	70	–	20	−0.208	4
Complete solidification	70	–	20	−0.167	5
Complete solidification	70	–	20	−0.046	18
Partial melting	20	55	20	0.2	8.83
Partial melting	20	57	20	0.2	9.17
Partial melting	20	62	20	0.2	10
Partial melting	20	67	20	0.2	10.83
Partial solidification	70	55	70	0.2	5.5
Partial solidification	70	50	70	0.2	6.33
Partial solidification	70	45	70	0.2	7.17
Partial solidification	70	40	70	0.2	8
Partial cycles	70	55-65-50-60-45-55	20	0.2	44

3.3. *Identification of PCM properties*

A numerical modelling of the fluxmeter bench presented in section 3.1 is required to identify some properties by inverse methods as explained below. The same numerical model is used in section 4 to simulate the experiments listed in Table 2. The numerical modelling is programmed with Python programming language. The modelling is carried out in 1D as the thermal exchanges in 2D are very limited inside the brick sample. Indeed, the heat loads applied to each face of the sample are symmetrical and the temperature applied is homogeneous on the sample surface. Moreover, convection motions in liquid

state are limited by the small thickness of the sample. As demonstrated by Thonon et al [21], convergence is reached with simulations performed with a 10 nodes spatial discretization along the PCM width and a time-step equals to the stability conditions of an explicit Euler method.

The identification process of PEG6000 thermal properties is achieved in four steps, explained in detail in the study of Thonon et al [21]. To reach a better accuracy, different thermal properties are identified for the solid and liquid phase [70].

As a first step, the liquid density is measured during the brick filling with the liquid PCM. The solid density is obtained once the PCM is fully solid inside the brick by measuring the height difference.

The second step consists of identifying the solid specific heat Cp_S, the liquid specific heat Cp_L and the latent heat L. These properties are obtained with energy balance calculations on the heat flux monitored experimentally between the PCM and the heat exchangers. Joulin et al [68] and Mazzeo et al [71] used similar methods, based on energy balance calculations, to obtain the PCM thermal properties. In this study, experiments on complete melting and solidification cycles with a duration of $18h$ are selected to calculate the energy balances. Indeed, it is easier to dissociate the sensible heat from the latent heat for slow heating and cooling rates. As the monitored solid sensible heat seems to depend on the temperature, also observed by Kou et al [59], a linear function is introduced to improve the model accuracy for $Cp_S(T)$ calculation. The reference solid specific heat value $Cp_S(T_0)$ and the temperature coefficient are determined by an inverse method on experiments with fully solid PCM.

The third step enables to identify by inverse method, from experiments where the PCM is fully solid or liquid, the solid thermal conductivity λ_S and the liquid thermal conductivity λ_L. The thermal resistances between the brick and fluxmeters, caused by an imperfect contact, are also determined in this third step. The identification process by inverse method consists of minimizing the sum of the squared errors, between the experiment and the numerical model, for two parameters: the heat flux and the temperature. This optimization on two objective functions is performed with a genetic algorithm (NSAG-II) computed with Platypus package from Python programming language. In theory, a single point should appear on the Pareto front of the multi-objectives optimization, because only one set of parameter is supposed to offer a perfect match between the numerical and experimental curves of heat flux and temperature. In reality, experimental results carried uncertainties and the numerical modelling of the fluxmeter bench includes simplifying assumptions. The Pareto front obtained is therefore composed by sets of parameters closed to each other. Indeed, as the two objectives are note opposite, an improvement on one objective leads to an improvement on the second objective. Even if the sets of parameters on the Pareto front are similar, the set of parameters the closest to the Utopia point is selected to characterize the PCM. The Utopia point is defined by the minimum of each objective function and presented Figure 7. The closest set of parameters from the Utopia point offers the best compromise between an accurate modelling of the temperature and the heat flux.

The fourth and final step identifies the parameters of the analytical model describing the thermodynamic state of the PCM. To achieve this, a second inverse method is carried out, with the same methodology than for the third step. The temperatures identified are specific to the phase change dynamic of PEG6000, and are defined in equations (9) and (10), as a modelling with two heat flux peaks is performed. A coefficient ε is integrated to the set of parameters to identify, this allows to take into account the latent heat distribution between materials/structures A and B (section 2.1). As explained in section 2.3, three identifications by inverse methods have to be performed in this fourth step: a first one to analytically model the melting process (referred with subscript $melt$), a second one for the analytical modelling of the supercooling and recalescence (referred with subscript SC), and a third one to identify the analytical model of the reference curve for cooling after a partial melting (referred with subscript Sol). Inverse methods on the analytical model of melting ($melt$) and supercooling (SC) are performed with the first and second sets of experiments with complete melting and solidification cycles, respectively. Inverse method to identify the cooling reference curve for partial melting (Sol) is performed with the third set of experiments after having implemented the analytical model of melting into the numerical model. For the identification of the supercooling and recalescence parameters, some of the temperatures describing the analytical model of the regular solidification are constrained. Indeed, as explained in section 2.2, the analytical modelling of the regular solidification is dependent of the PCM temperature at the end of the recalescence. Therefore, it requires a numerical solving to ensure a continuity of the liquid fraction and a balanced enthalpy, regardless of the boundary conditions influencing the recalescence process. However, still concerning the identification of parameters for supercooling and recalescence, other parameters have to be identified, such as the constants defining the start and the duration of the recalescence in equations (11) and (15), respectively.

Figure 7 presents the Pareto front obtained after the identification of the analytical model related to the melting phase change of PEG6000. Figure 8 shows the low dispersion of the sets of parameters of the Pareto front. Only the parameter of latent heat distribution ε_{melt} shows a slightly dispersion with the first and third quarter at approximatively 5% of the normalized mean value. Table 3 details the results obtained for each step of the identification process of PEG6000 properties.

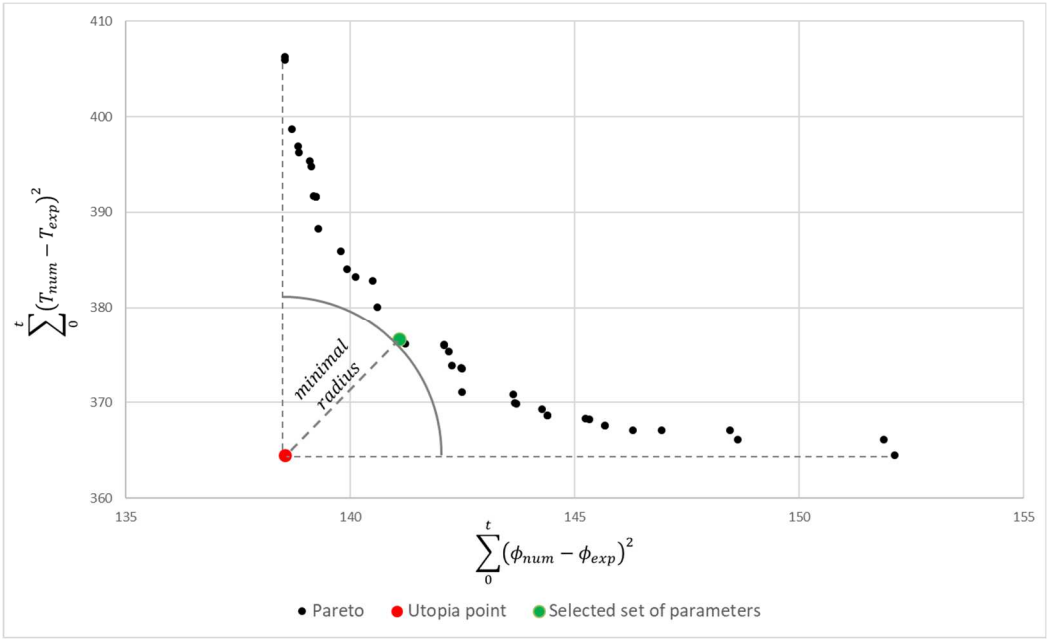

Figure 7: Pareto front obtained after the optimization process on melting experiments

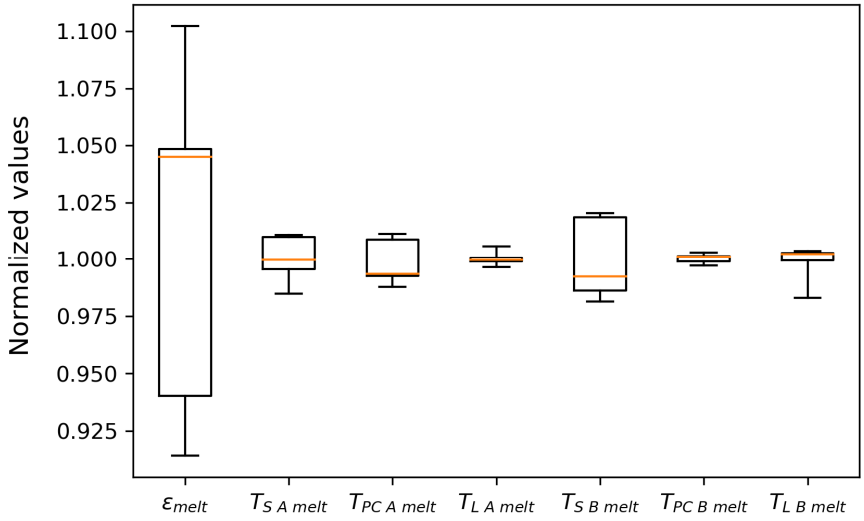

Figure 8: Boxplot (minimal value, first quartile, median value, third quartile and maximal value) of the Pareto sets of parameters normalized by the mean value after the optimization process on the set of experiments on complete melting.

Table 3: PEG6000 properties determined according to the four steps of the identification process and the three analytical models identified

Step	**PEG 6000 Properties**		
I	$\rho_S = 1200 \quad kg.m^{-3}$ $\rho_L = 1070 \quad kg.m^{-3}$		
II	$Cp_S(T) = 1450 + 20 * (T - 273) \quad J.kg.K^{-1}$ $Cp_L = 2450 \quad J.kg.K^{-1}$ $L = 172500 \quad J.kg^{-1}$		
III	$\lambda_S = 0.35 \quad W.m^{-1}.K^{-1}$ $\lambda_L = 0.41 \quad W.m^{-1}.K^{-1}$		
IV	Complete melting $\varepsilon_{melt} = 0.38$ $T_{S\,A\,melt} = 49.0\,°C$	Complete solidification (supercooling + recalescence) $K_1 = 53.0\,°C$ $K_2 = -0.0102$	Reference cooling curve (for cooling after partial melting) $\varepsilon_{sol} = 0.31$ $T_{S\,A\,sol} = 35.3°C$

$T_{PC\ A\ melt} = 57.8\ °C$	$K_3 = 4664\ s$	$T_{PC\ A\ sol} = 52.1°C$
$T_{L\ A\ melt} = 59.7\ °C$	$K_4 = -0.517$	$T_{L\ A\ sol} = 59.7°C$
$T_{S\ B\ melt} = 58.3\ °C$	$\varepsilon_{SC} = 0.66$	$T_{S\ B\ sol} = 49.8°C$
$T_{PC\ B\ melt} = 60.9\ °C$	$T_{S\ 1\ SC} = 32\ °C$	$T_{PC\ B\ sol} = 54.0°C$
$T_{L\ B\ melt} = 67.1\ °C$	$K_5 = 0.016\ °C$	$T_{L\ B\ sol} = 60.8°C$

The values of specific heat identified in step II are slightly higher than those obtained by Kou et al [59] by DSC. Concerning thermal conductivity of the solid phase, the results are similar than those presented by Kou et al [59] and Tang et al [72]. For the liquid phase, the slightly higher value of thermal conductivity might be explained – as it is frequently made in several studies [37,39] – by the convection cells, even if limited, which intensify the heat transfers. In overall, the latent heat and the melting temperature are in agreements with the DSC results from various study [40,45,59,72].

4. Results and discussion

4.1. Analytical modelling of PEG6000

Identification of PEG6000 properties and of the parameters of the analytical models involved in the numerical modelling presented in this article enables to describe the evolution of the liquid fraction $f(T)$, the effective heat capacity $C_{eff}(T)$ and the enthalpy $H(T)$ for the different thermal processes studied: complete melting, complete solidification, partial melting and partial solidification.

First, the behavior of PEG6000 during complete melting is characterized by $f(T)$, $C_{eff}(T)$ and $H(T)$ in red in Figure 9. Concerning melting, the analytical formulation is unique regardless of the heating rate of the PCM. Numerical and experimental results are compared for different heating rates in section 4.2

For a complete solidification, with supercooling and a recalescence process, the curves of $f(T)$, $C_{eff}(T)$ and $H(T)$ are dependent on the cooling rate and are presented in blue in Figure 9. As explained in section 2.2, the cooling rate influences the degree of supercooling, the amount of latent heat release, and the duration of the recalescence. Analytical representation of $f(T)$, $C_{eff}(T)$ and $H(T)$, for supercooling and recalescence, are currently rarely presented in the literature. Section 4.3 compares the numerical and experimental results for four different cooling rates.

As detailed in section 2.3, modelling of partial melting requires to use a cooling reference curve specific to the case where the PCM is cooled before reaching a fully liquid state. Indeed, the crystals still present inside the PCM, at the interruption of the heating cycle, do not enable to maintain a metastable state during the cooling cycle. The reference curve related to this particular configuration is presented by the graphs $f(T)$, $C_{eff}(T)$ and $H(T)$ in green in Figure 9. Section 4.4 details the results for partial melting cycles with different temperature plateaus.

Finally, the case of partial solidification is studied, where the PCM is reheated before reaching a fully solid state. The thermal behavior of the PCM during the temperature rise is described by the "curve scale" hysteresis model defined by equation (20). Section 4.5 presents the results for partial solidification cycles with different temperature plateaus.

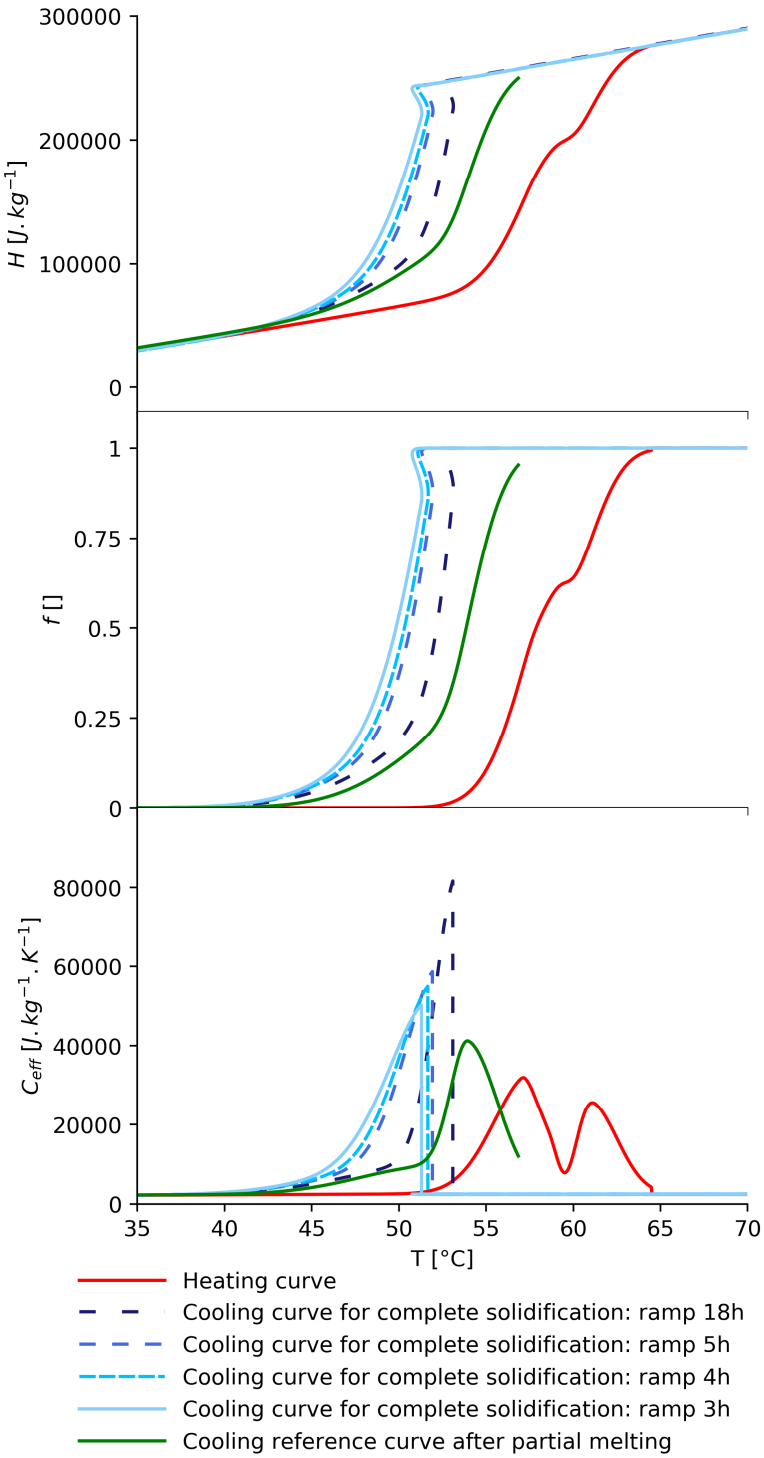

Figure 9: Evolution of enthalpy (top), liquid fraction (middle) and effective heat capacity (bottom) for PEG6000

4.2. Complete melting for different heating rates

Comparison between experimental and numerical results for complete melting cycles with different heating rates is presented with Figure 10. Temperature T_{Hx} represents the heat exchanger temperature which corresponds to the heat rate β applied to the sample. During the melting cycle, a double plateau of temperature $T_{PCM\ exp}$ is observed, for all the heating rates, with the thermocouple located at the middle of the sample. But, only for the $18h$ heating ramp, this double temperature plateau $T_{PCM\ exp}$ is translated into a double heat flux peak F_{exp}. This means that it is essential to monitor both the temperature and the heat flux on different heating rates to get a complete experimental characterization of the sample. Indeed, heat flux measurement with fluxmeters, on the outer walls of the PMMA brick, evaluates the global thermal behavior of the PCM. However, local phenomena, such as a double temperature plateau for PEG6000, might remain unseen for fast heating rates.

On the contrary, temperature measurement with thermocouples is local, and the thermal behavior observed locally might not be representative for the global thermal behavior of the entire PCM sample. Furthermore, it appears necessary to model two materials/structures, as defined by equations (9) and (10), to represent accurately the temperature plateaus during the melting cycles of PEG6000.

Overall, as shown with Figure 10, the temperature is correctly estimated by the model for the four heating rates tested. The results are also satisfactory concerning the heat flux modelling, even if the modelling of the double heat flux peaks of the $18h$ heating ramp remains slightly less accurate.

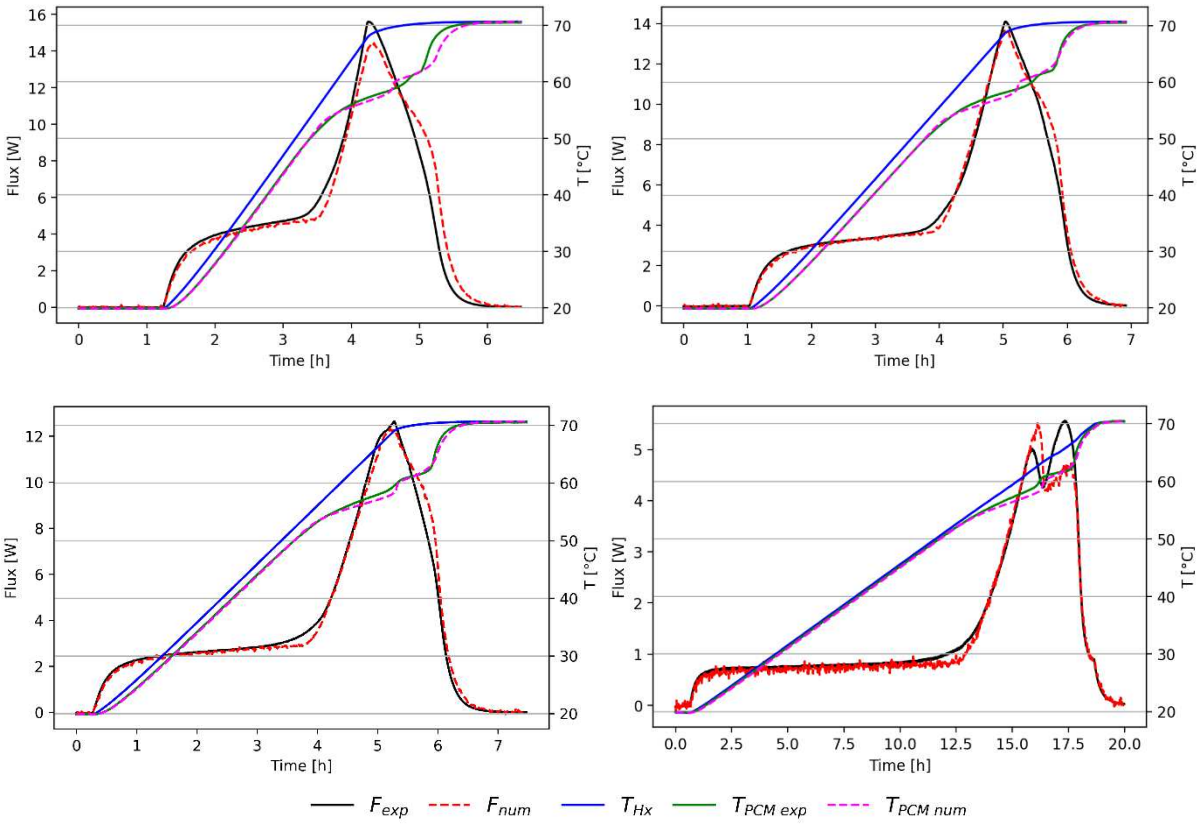

Figure 10: Experimental and numerical results for complete melting in 3h (top left), 4h (top right), 5h (bottom left) and 18h (bottom right)

4.3. Complete solidification for different cooling rates

Figure 11 presents the results for complete solidification cycles of PEG6000 for different cooling rates. The values of the parameters characterizing the supercooling and the recalescence processes are presented in Table 4 for each cooling rate. For the four studied cooling rates, the modelling of supercooling and recalescence processes are in good agreement with the experimental results of heat flux and temperature. The behavior laws used to determine temperature $T_{reca\ start}(\beta)$ with equation (11), the heat release duration $\Delta t_{reca}(\beta)$ with equation (15), and the heat release profile $q_{reca}(t)$ with equation (16), seem to be valid for the studied cooling rate range. As temperature $T_{reca\ start}$ turns to be only slightly dependent of the cooling rate of PEG6000, it is therefore not possible to generalize the power law formulation of equation (11) for PCM where the cooling rate influences significantly the supercooling degree.

Modelling the end of the solidification, after the recalescence process, thanks to a classic analytical modelling is relevant for PEG6000, with only a short time-gap between experimental and numerical heat flux curves. The effective heat capacity jump, represented with the blue curves Figure 9, enables to model the establishment of a quasi-plateau of temperature at the end of the recalescence process.

Table 4: Supercooling parameters for each cooling rate

Experiment		**Supercooling parameters**				
Duration	***β***	$T_{reca\ start}$	Δt_{reca}	$T_{reca\ end}$	$f_{reca\ end}$	Q_{reca}

$[h]$	$[K.min^{-1}]$	$[°C]$	$[s]$	$[°C]$	$[-]$	$[J.kg^{-1}]$
3	-0.278	51.50	1087	51.87	0.839	27 772
4	-0.208	51.65	1263	52.18	0.840	27 600
5	-0.167	51.76	1404	52.45	0.842	27 255
18	-0.046	52.48	2831	53.28	0.852	25 530

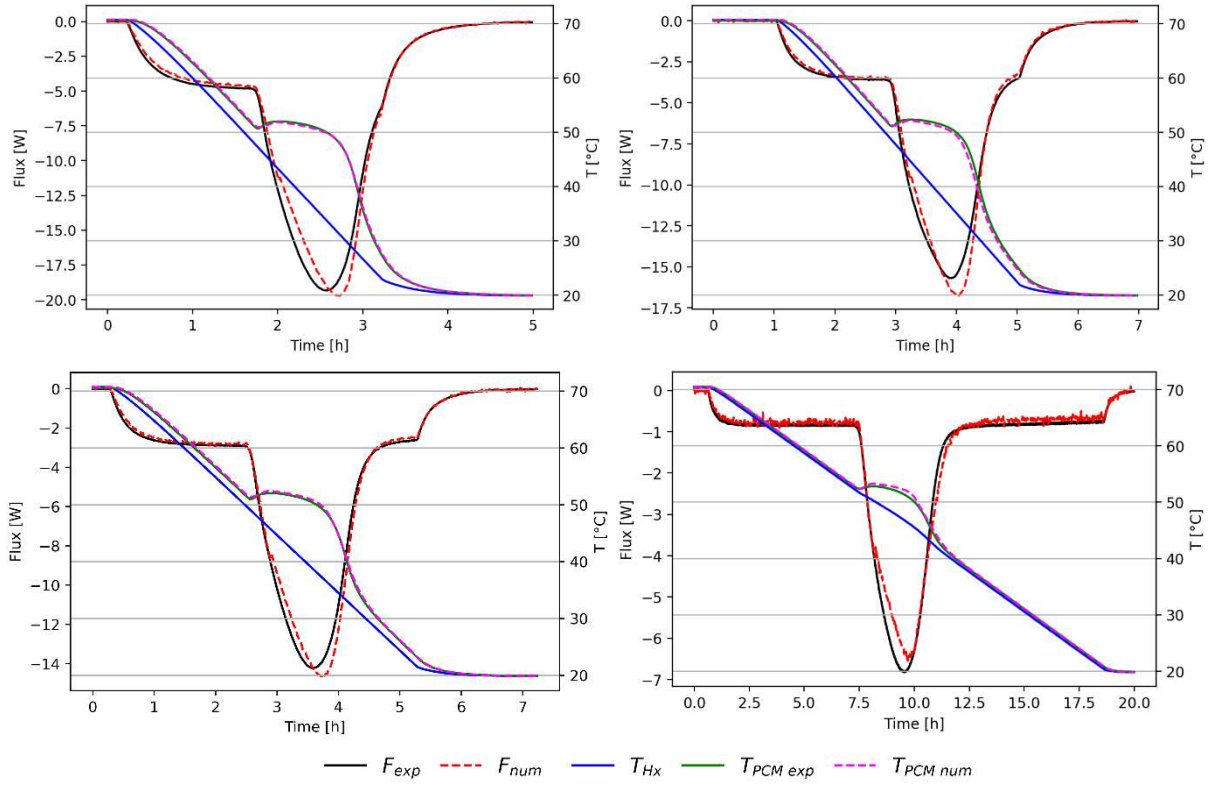

Figure 11: Experimental and numerical results for complete solidification in 3h (top left), 4h (top right), 5h (bottom left) and 18h (bottom right)

4.4. Partial melting for different temperatures

Figure 12 shows the results of partial melting cycles modelling for temperature plateaus of 55-57-62-67$°C$. The numerical model developed does not reproduce correctly the thermal behavior, with a strong overestimation of the heat flux for the temperature plateaus of 57$°C$, 62$°C$ and 67$°C$. Moreover, for the configuration with the 67$°C$ temperature plateau, it seems that the model overestimates the heat flux during the heating ramp, before the temperature plateau, while the modelling of the nearly same heating rate for complete melting was correct in Figure 10. This different thermal behavior, between complete and partial melting cycles, might be explained by the shape of the preceding storage process as observed by different studies on PEG solidification [43–45]. Experiments on partial melting cycles where carried out one after the other, this means experiments with temperature plateaus of 57-62-67$°C$ where preceded by partial melting experiments. To our best knowledge, for LHTES applications, no study focuses specifically on the influence of a partial melting cycle on the crystalline structure of PEG6000, or more generally on polymers, and the impact of the crystalline structure on the melting process.

As illustrated by Figure 12, the error of modelling, during the partial melting cycles for temperature plateaus of 57-62$°C$, also appears for the solidification. Indeed, in order to ensure an energy balance at equilibrium between the initial and final state at 20$°C$, the surplus of energy modelled during the partial melting has to be released during the solidification. As the modelling error might come from complex phenomena specific to polymers [43–45] which are not modelled, it is difficult to evaluate the accuracy of the hysteresis model "curve scale" during the cooling cycle for temperature plateaus of 57-62$°C$. Finally, supercooling and recalescence are observed for the cooling cycle of the experiment with the temperature plateau of 67$°C$. This configuration is close to a complete melting cycle with a liquid fraction close to 1 during the temperature plateau. As detailed before, the modelled PCM follows a supercooled behavior, with a metastable state, if the liquid fraction reaches 0.95, as it is the case for the 67$°C$ temperature plateau.

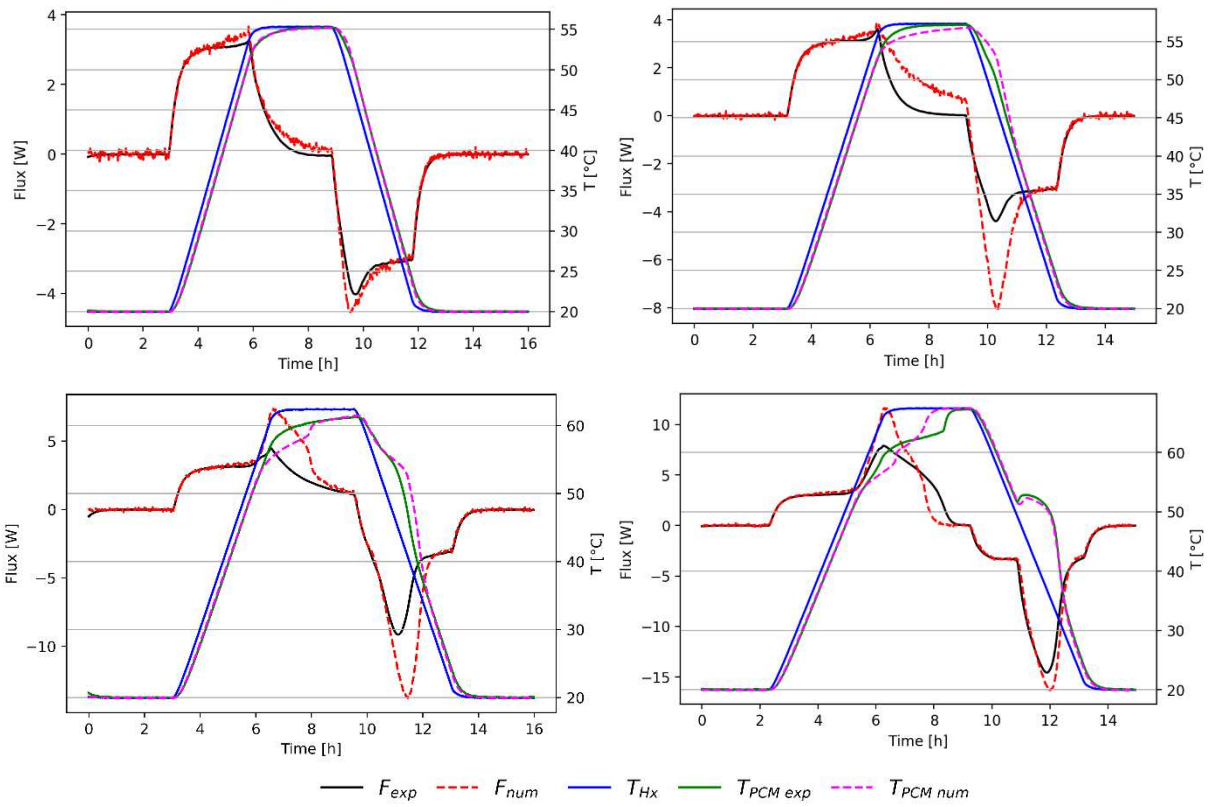

Figure 1: Experimental and numerical results for partial melting with temperature plateau at 55°C (top left), 57°C (top right), 62°C (bottom left) and 67°C (bottom right)

4.5. Partial solidification for different temperatures

A partial solidification is defined by a reheating of the PCM before reaching a fully solid state. In this configuration, the hysteresis model "curve scale" with equation (20) is selected to model the reheating of the PCM. Figure 13 details the results for partial solidification cycles with temperature plateaus of $55\text{-}50\text{-}45\text{-}40°C$.

For the temperature plateau at $55°C$, the metastable state is not broken and only sensible heat is exchanged. The temperature plateau at $50°C$ presents a particular configuration where the crystallization starts during the establishment of the temperature plateau. This does not lead to a significant rise of the PCM temperature, but to a slow kinetic of crystallisation because the PCM temperature does not return to $50°C$ at the end of the $3h$ plateau. In this specific configuration, the numerical modelling remains satisfactory, even though the behavior laws of recalescence have been identified for temperature ramps and not temperature plateaus. Concerning temperature plateaus of $45°C$ and $40°C$, the thermal behavior is quite similar than for complete solidification cycles, and the hysteresis model "curve scale" enables an accurate modelling of the heat flux and temperature during the reheating cycle.

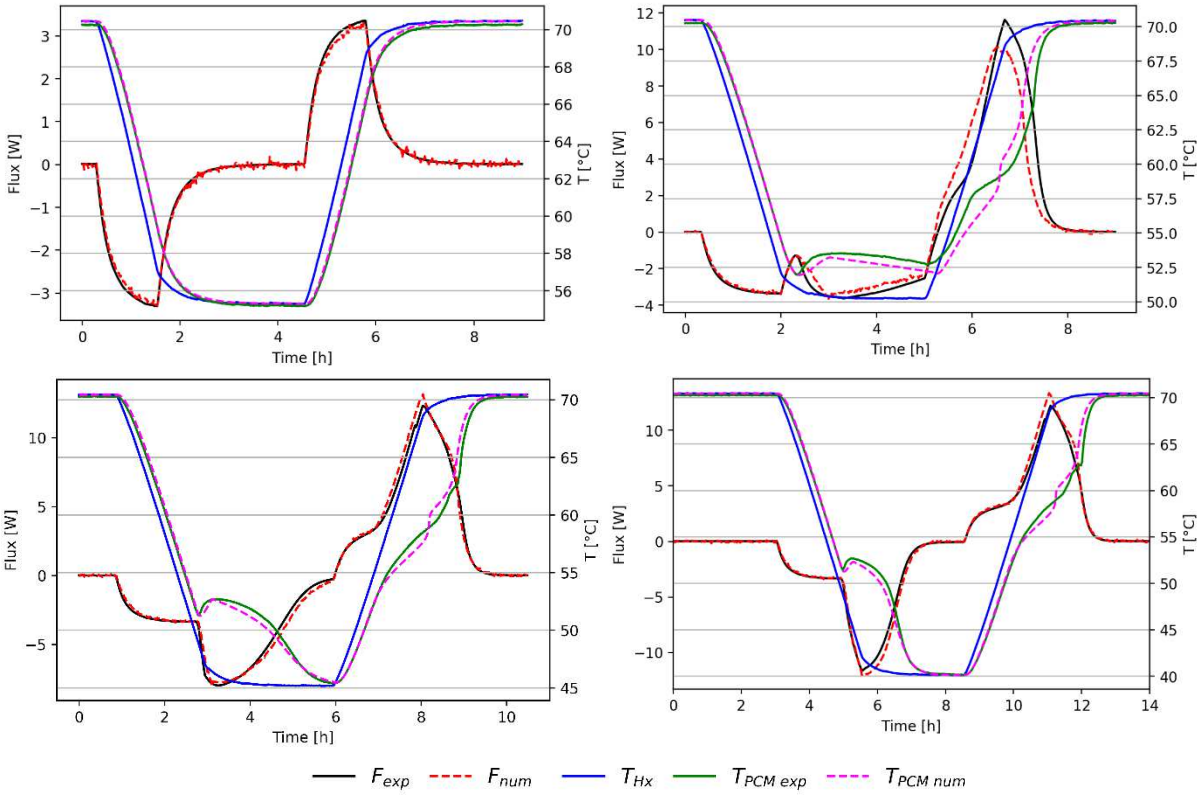

Figure 13: Experimental and numerical results for partial solidification with temperature plateau at 55°C (top left), 50°C (top right), 45°C (bottom left) and 40°C (bottom right)

4.6. Partial cycles of melting and solidification

The last experiment conducted consists of a serie of partial cycles to evaluate the accuracy and robustness of the model by getting closer to the functioning of a LHTES. Starting from a temperature at $70°C$, a succession of temperature plateaus at $55\text{-}65\text{-}50\text{-}60\text{-}45\text{-}55°C$ are conducted before ending at $20°C$. Numerical results are compared to experimental ones on Figure 14.

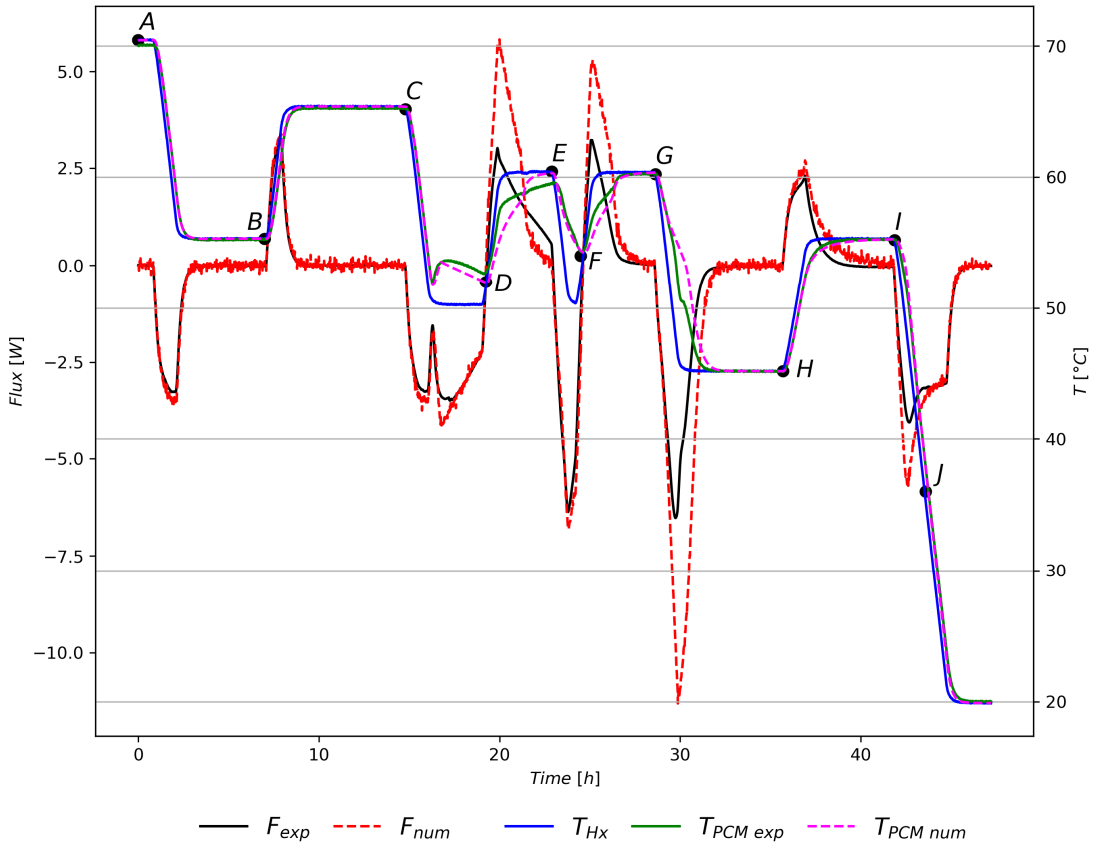

Figure 14: Experimental and numerical results for partial phase change cycles

As for the experiments with partial melting cycles, where the initial state of the crystalline structure influences the melting dynamic, the numerical modelling is not correct for the partial melting cycles with a temperature plateau of $60°C$ at $20h$ and $25h$. The surplus of heat accumulated during these two partial melting cycles is then removed during the cooling ramp leading to the temperature plateau at $45°C$ around $30h$. Otherwise, results are accurate for the other cycling phases. Figure 15 shows the evolution of the numerical liquid fraction during the experiment with the different points of transition between heating and cooling cycles.

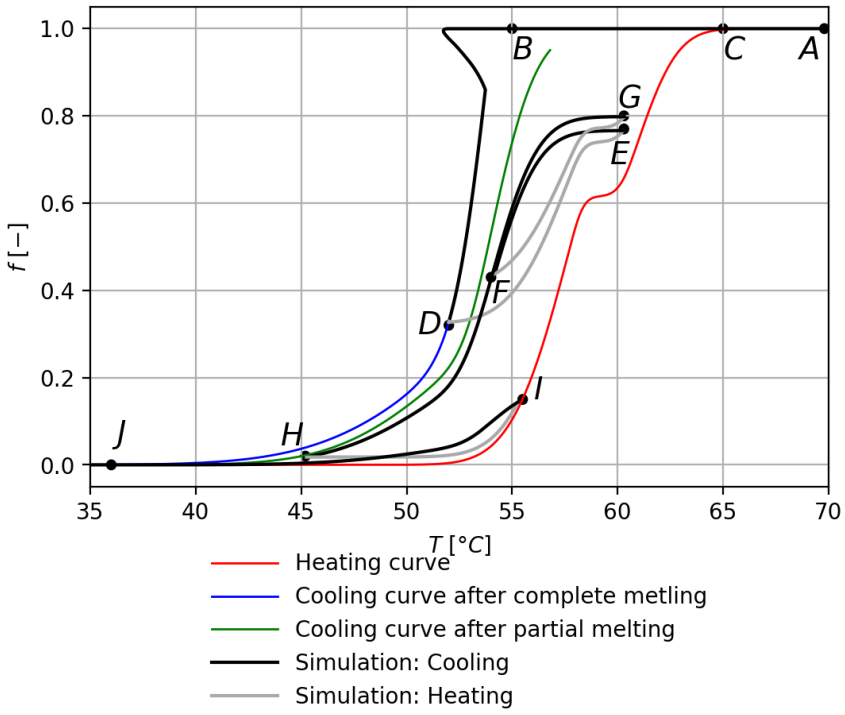

Figure 15: Evolution of the liquid fraction for the partial phase change cycles experiment

5. Conclusion and outlooks

The objective of this article is to model analytically a PCM experiencing supercooling for complete and partial phase change cycles. The main contribution of this study is :

- To consider both supercooling and phase change hysteresis for various thermal processes. The developed method models the three phenomenological criteria observed during the solidification of a PCM experiencing supercooling: the metastable state, the recalescence process and the regular solidification.
- To take into account the influence of the cooling rate on the recalescence process, which is currently rarely considered.
- To ensure a balanced heat budget and a continuity of the liquid fraction, enthalpy and temperatures during the solidification cycle
- To represent analytically the liquid fraction, the effective heat capacity, and the enthalpy, during the different step of the cooling cycle, which is rarely presented in the existing literature.

The PCM studied is PEG6000, a polymer offering interesting properties for DHW storage. Experimental validation of the model is performed with a brick filled with PCM in order to get closer to the real behavior of a LHTES. A complete thermal experimental characterisation of the PCM is achieved by measuring both the PCM temperature and the heat flux on the outer surface of the sample.

Comparison between experimental and numerical results show:

- A good agreement for complete phase change cycles for various heating/cooling rates. Modelling two materials/structures is relevant, especially for complete melting. The behavior laws, evaluating the influence of the cooling rate on the supercooling and recalescence processes, are validated on the cooling rate range tested
- A good agreement for partial solidification cycles for different temperature plateaus. The hysteresis model “curve scale” is performant and describes correctly the thermal behavior of PEG6000
- An incomplete validation of the model for partial melting. The numerical model does not succeed to reproduce the heat transfers within the PCM during the heating cycles if the previous cycle was a partial melting cycle. In order to keep a balanced heat budget, the error of modelling from the partial heating cycle is also present during the cooling cycle.

This study also raises perspectives for research on supercooling modelling for polymers. Indeed, the phase change dynamic of PEG6000, and of polymers more generally, seems to be strongly influenced by the structure of the crystalline solid state,

which depends on the solidification conditions. To this day, the influence of the solidification conditions on the crystalline structure, and its impact on the melting dynamic, is rarely studied for LHTES applications. Introducing an analytical formulation, depending on the previous heating and cooling cycles, to define the crystalline state might be a solution to improve the accuracy of PEG6000 modelling. It would also be interested to test the developed method to model the supercooling and the recalescence processes for a different kind of PCM, such as sugar alcohols or salt hydrates for example.

Declaration of Competing Interest

The authors declare that they have no known competing financial interests or personal relationships that could have appeared to influence the work reported in this paper.

Acknowledgements

This study takes part in the EUROPA project funded by the ANR (French National Research Agency).

References

[1] H. Nazir, M. Batool, F.J. Bolivar Osorio, M. Isaza-Ruiz, X. Xu, K. Vignarooban, P. Phelan, Inamuddin, A.M. Kannan, Recent developments in phase change materials for energy storage applications: A review, International Journal of Heat and Mass Transfer. 129 (2019) 491–523. https://doi.org/10.1016/j.ijheatmasstransfer.2018.09.126.

[2] A. Arnault, F. Mathieu-Potvin, L. Gosselin, Internal surfaces including phase change materials for passive optimal shift of solar heat gain, International Journal of Thermal Sciences. 49 (2010) 2148–2156. https://doi.org/10.1016/j.ijthermalsci.2010.06.021.

[3] F. Kuznik, D. David, K. Johannes, J.-J. Roux, A review on phase change materials integrated in building walls, Renewable and Sustainable Energy Reviews. 15 (2011) 379–391. https://doi.org/10.1016/j.rser.2010.08.019.

[4] H. Ye, L. Long, H. Zhang, R. Zou, The performance evaluation of shape-stabilized phase change materials in building applications using energy saving index, Applied Energy. 113 (2014) 1118–1126. https://doi.org/10.1016/j.apenergy.2013.08.067.

[5] X. Sun, Q. Zhang, M.A. Medina, K.O. Lee, Energy and economic analysis of a building enclosure outfitted with a phase change material board (PCMB), Energy Conversion and Management. 83 (2014) 73–78. https://doi.org/10.1016/j.enconman.2014.03.035.

[6] M.H. Abokersh, M. Osman, O. El-Baz, M. El-Morsi, O. Sharaf, Review of the phase change material (PCM) usage for solar domestic water heating systems (SDWHS): Use of phase change material in domestic solar water heating systems, International Journal of Energy Research. 42 (2018) 329–357. https://doi.org/10.1002/er.3765.

[7] N. Beaupere, U. Soupremanien, L. Zalewski, Nucleation triggering methods in supercooled phase change materials (PCM), a review, Thermochimica Acta. 670 (2018) 184–201. https://doi.org/10.1016/j.tca.2018.10.009.

[8] A. Safari, R. Saidur, F.A. Sulaiman, Y. Xu, J. Dong, A review on supercooling of Phase Change Materials in thermal energy storage systems, Renewable and Sustainable Energy Reviews. 70 (2017) 905–919. https://doi.org/10.1016/j.rser.2016.11.272.

[9] D. Clausse, J.-P. Dumas, Supercooling, Crystallization and Melting within Emulsions and Divided Systems: Mass, Heat Transfers and Stability, Bentham Science Publishers Ltd., 2016.

[10] A. Nejman, M. Cieślak, The impact of the heating/cooling rate on the thermoregulating properties of textile materials modified with PCM microcapsules, Applied Thermal Engineering. 127 (2017) 212–223. https://doi.org/10.1016/j.applthermaleng.2017.08.037.

[11] A. Mollova, R. Androsch, D. Mileva, C. Schick, A. Benhamida, Effect of Supercooling on Crystallization of Polyamide 11, Macromolecules. 46 (2013) 828–835. https://doi.org/10.1021/ma302238r.

[12] B. Sandnes, J. Rekstad, Supercooling salt hydrates: Stored enthalpy as a function of temperature, Solar Energy. 80 (2006) 616–625. https://doi.org/10.1016/j.solener.2004.11.014.

[13] L. Desgrosseilliers, P. Allred, D. Groulx, M.A. White, Determination of enthalpy–temperature–composition relations in incongruent-melting phase change materials, Applied Thermal Engineering. 61 (2013) 193–197. https://doi.org/10.1016/j.applthermaleng.2013.07.019.

[14] N. Beaupere, U. Soupremanien, L. Zalewski, Experimental measurements of the residual solidification duration of a supercooled sodium acetate trihydrate, International Journal of Thermal Sciences. 158 (2020) 106544. https://doi.org/10.1016/j.ijthermalsci.2020.106544.

[15] A. García-Romero, G. Diarce, J. Ibarretxe, A. Urresti, J.M. Sala, Influence of the experimental conditions on the subcooling of Glauber's salt when used as PCM, Solar Energy Materials and Solar Cells. 102 (2012) 189–195. https://doi.org/10.1016/j.solmat.2012.03.003.

[16] T. Adachi, D. Daudah, G. Tanaka, Effects of Supercooling Degree and Specimen Size on Supercooling Duration of Erythritol, ISIJ International. 54 (2014) 2790–2795. https://doi.org/10.2355/isijinternational.54.2790.

[17] G. Zhou, Y. Xiang, Experimental investigations on stable supercooling performance of sodium acetate trihydrate PCM for thermal storage, Solar Energy. 155 (2017) 1261–1272. https://doi.org/10.1016/j.solener.2017.07.073.

[18] M. Faucheux, G. Muller, M. Havet, A. LeBail, Influence of surface roughness on the supercooling degree: Case of selected water/ethanol solutions frozen on aluminium surfaces, International Journal of Refrigeration. 29 (2006) 1218–1224. https://doi.org/10.1016/j.ijrefrig.2006.01.002.

[19] J.-P. Dumas, S. Gibout, L. Zalewski, K. Johannes, E. Franquet, S. Lassue, J.-P. Bédécarrats, P. Tittelein, F. Kuznik, Interpretation of calorimetry experiments to characterise phase change materials, International Journal of Thermal Sciences. 78 (2014) 48–55. https://doi.org/10.1016/j.ijthermalsci.2013.11.014.
[20] J.P. Dumas, S. Gibout, P. Cézac, E. Franquet, New theoretical determination of latent heats from DSC curves, Thermochimica Acta. 670 (2018) 92–106. https://doi.org/10.1016/j.tca.2018.10.011.
[21] M. Thonon, G. Fraisse, L. Zalewski, M. Pailha, Towards a better analytical modelling of the thermodynamic behaviour of phase change materials, Journal of Energy Storage. 32 (2020) 101826. https://doi.org/10.1016/j.est.2020.101826.
[22] E. Franquet, S. Gibout, J.-P. Bédécarrats, D. Haillot, J.-P. Dumas, Inverse method for the identification of the enthalpy of phase change materials from calorimetry experiments, Thermochimica Acta. 546 (2012) 61–80. https://doi.org/10.1016/j.tca.2012.07.015.
[23] J. Bony, S. Citherlet, Numerical model and experimental validation of heat storage with phase change materials, Energy and Buildings. 39 (2007) 1065–1072. https://doi.org/10.1016/j.enbuild.2006.10.017.
[24] E. Günther, H. Mehling, S. Hiebler, Modeling of subcooling and solidification of phase change materials, Modelling and Simulation in Materials Science and Engineering. 15 (2007) 879–892. https://doi.org/10.1088/0965-0393/15/8/005.
[25] C. Le Bot, D. Delaunay, Rapid solidification of indium: Modeling subcooling, Materials Characterization. 59 (2008) 519–527. https://doi.org/10.1016/j.matchar.2007.03.010.
[26] A.Y. Uzan, Y. Kozak, Y. Korin, I. Harary, H. Mehling, G. Ziskind, A novel multi-dimensional model for solidification process with supercooling, International Journal of Heat and Mass Transfer. 106 (2017) 91–102. https://doi.org/10.1016/j.ijheatmasstransfer.2016.10.046.
[27] X. Jin, H. Hu, X. Shi, X. Zhou, L. Yang, Y. Yin, X. Zhang, A new heat transfer model of phase change material based on energy asymmetry, Applied Energy. 212 (2018) 1409–1416. https://doi.org/10.1016/j.apenergy.2017.12.103.
[28] T. Davin, B. Lefez, A. Guillet, Supercooling of phase change: A new modeling formulation using apparent specific heat capacity, International Journal of Thermal Sciences. 147 (2020) 106121. https://doi.org/10.1016/j.ijthermalsci.2019.106121.
[29] C. Rathgeber, L. Miró, L.F. Cabeza, S. Hiebler, Measurement of enthalpy curves of phase change materials via DSC and T-History: When are both methods needed to estimate the behaviour of the bulk material in applications?, Thermochimica Acta. 596 (2014) 79–88. https://doi.org/10.1016/j.tca.2014.09.022.
[30] D. Mazzeo, EnergyPlus, IDA ICE and TRNSYS predictive simulation accuracy for building thermal behaviour evaluation by using an experimental campaign in solar test boxes with and without a PCM module, (2020) 30.
[31] L. Liu, X. Zhang, X. Xu, Y. Zhao, S. Zhang, The research progress on phase change hysteresis affecting the thermal characteristics of PCMs: A review, Journal of Molecular Liquids. 317 (2020) 113760. https://doi.org/10.1016/j.molliq.2020.113760.
[32] L. Klimeš, P. Charvát, M. Mastani Joybari, M. Zálešák, F. Haghighat, K. Panchabikesan, M. El Mankibi, Y. Yuan, Computer modelling and experimental investigation of phase change hysteresis of PCMs: The state-of-the-art review, Applied Energy. 263 (2020) 114572. https://doi.org/10.1016/j.apenergy.2020.114572.
[33] A. Fateh, F. Klinker, M. Brütting, H. Weinläder, F. Devia, Numerical and experimental investigation of an insulation layer with phase change materials (PCMs), Energy and Buildings. 153 (2017) 231–240. https://doi.org/10.1016/j.enbuild.2017.08.007.
[34] K. Kumarasamy, J. An, J. Yang, E.-H. Yang, Novel CFD-based numerical schemes for conduction dominant encapsulated phase change materials (EPCM) with temperature hysteresis for thermal energy storage applications, Energy. 132 (2017) 31–40. https://doi.org/10.1016/j.energy.2017.05.054.
[35] F. Goia, G. Chaudhary, S. Fantucci, Modelling and experimental validation of an algorithm for simulation of hysteresis effects in phase change materials for building components, Energy and Buildings. 174 (2018) 54–67. https://doi.org/10.1016/j.enbuild.2018.06.001.
[36] B. Delcroix, M. Kummert, A. Daoud, Thermal Behavior Mapping of a Phase Change Material Between the Heating and Cooling Enthalpy-temperature Curves, Energy Procedia. 78 (2015) 225–230. https://doi.org/10.1016/j.egypro.2015.11.612.
[37] T. Barz, A. Sommer, Modeling hysteresis in the phase transition of industrial-grade solid/liquid PCM for thermal energy storages, International Journal of Heat and Mass Transfer. 127 (2018) 701–713. https://doi.org/10.1016/j.ijheatmasstransfer.2018.08.032.
[38] Y. Ivshin, T.J. Pence, A constitutive model for hysteretic phase transition behavior, Int. J. Engn Sci. 32 (1994) 681–704.
[39] T. Barz, J. Emhofer, K. Marx, G. Zsembinszki, L.F. Cabeza, Phenomenological modelling of phase transitions with hysteresis in solid/liquid PCM, Journal of Building Performance Simulation. 12 (2019) 770–788. https://doi.org/10.1080/19401493.2019.1657953.
[40] R.K. Sharma, P. Ganesan, V.V. Tyagi, T.M.I. Mahlia, Accelerated thermal cycle and chemical stability testing of polyethylene glycol (PEG) 6000 for solar thermal energy storage, Solar Energy Materials and Solar Cells. 147 (2016) 235–239. https://doi.org/10.1016/j.solmat.2015.12.023.
[41] M. Bilardo, G. Fraisse, M. Pailha, E. Fabrizio, Modelling and performance analysis of a new concept of integral collector storage (ICS) with phase change material, Solar Energy. 183 (2019) 425–440. https://doi.org/10.1016/j.solener.2019.03.032.
[42] G. Strobl, Crystallization and melting of bulk polymers: New observations, conclusions and a thermodynamic scheme, Progress in Polymer Science. 31 (2006) 398–442. https://doi.org/10.1016/j.progpolymsci.2006.01.001.

[43] J.M. Ginés, M.J. Arias, J.R. Moyano, P.J. Sánchez-Soto, Thermal investigation of crystallization of polyethylene glycols in solid dispersions containing oxazepam, International Journal of Pharmaceutics. 143 (1996) 247–253. https://doi.org/10.1016/S0378-5173(96)04702-3.
[44] J.K. Hobbs, In situ atomic force microscopy of the melting of melt-crystallized polyethylene, Polymer. 47 (2006) 5566–5573. https://doi.org/10.1016/j.polymer.2005.02.133.
[45] S. Verheyen, P. Augustijns, R. Kinget, G. Van den Mooter, Melting behavior of pure polyethylene glycol 6000 and polyethylene glycol 6000 in solid dispersions containing diazepam or temazepam: a DSC study, Thermochimica Acta. 380 (2001) 153–164. https://doi.org/10.1016/S0040-6031(01)00666-9.
[46] H. Hu, S.A. Argyropoulos, Mathematical modelling of solidification and melting: a review, Modelling and Simulation in Materials Science and Engineering. 4 (1996) 371–396. https://doi.org/10.1088/0965-0393/4/4/004.
[47] D. Zhang, A.S. Fung, O. Siddiqui, Dept. of Mechanical and Industrial Engineering, Ryerson University, Toronto, Canada, T Ime. (2007) 6.
[48] A. Bastani, F. Haghighat, J. Kozinski, Designing building envelope with PCM wallboards: Design tool development, Renewable and Sustainable Energy Reviews. 31 (2014) 554–562. https://doi.org/10.1016/j.rser.2013.12.031.
[49] M. Nabavitabatabayi, F. Haghighat, A. Moreau, P. Sra, Numerical analysis of a thermally enhanced domestic hot water tank, Applied Energy. 129 (2014) 253–260. https://doi.org/10.1016/j.apenergy.2014.04.081.
[50] M. Liu, Y. Sun, F. Bruno, A review of numerical modelling of high-temperature phase change material composites for solar thermal energy storage, Journal of Energy Storage. 29 (2020) 101378. https://doi.org/10.1016/j.est.2020.101378.
[51] K. Darkwa, P.W. O'Callaghan, Simulation of phase change drywalls in a passive solar building, Applied Thermal Engineering. 26 (2006) 853–858. https://doi.org/10.1016/j.applthermaleng.2005.10.007.
[52] B. Xie, W. Cheng, Z. Xu, Studies on the effect of shape-stabilized PCM filled aluminum honeycomb composite material on thermal control, International Journal of Heat and Mass Transfer. 91 (2015) 135–143. https://doi.org/10.1016/j.ijheatmasstransfer.2015.07.108.
[53] P. Tan, M. Brütting, S. Vidi, H.-P. Ebert, P. Johansson, H. Jansson, A.S. Kalagasidis, Correction of the enthalpy–temperature curve of phase change materials obtained from the T-History method based on a transient heat conduction model, International Journal of Heat and Mass Transfer. 105 (2017) 573–588. https://doi.org/10.1016/j.ijheatmasstransfer.2016.10.001.
[54] M. Brütting, S. Vidi, F. Hemberger, H.P. Ebert, Dynamic T-History method - A dynamic thermal resistance for the evaluation of the enthalpy-temperature curve of phase change materials, Thermochimica Acta. 671 (2019) 161–169. https://doi.org/10.1016/j.tca.2018.10.030.
[55] H. Yang, Y. He, Solving heat transfer problems with phase change via smoothed effective heat capacity and element-free Galerkin methods, International Communications in Heat and Mass Transfer. 37 (2010) 385–392. https://doi.org/10.1016/j.icheatmasstransfer.2009.12.002.
[56] E. Franquet, S. Gibout, P. Tittelein, L. Zalewski, J.-P. Dumas, Experimental and theoretical analysis of a cement mortar containing microencapsulated PCM, Applied Thermal Engineering. 73 (2014) 32–40. https://doi.org/10.1016/j.applthermaleng.2014.06.053.
[57] R. Paukkeri, A. Lehtinen, Thermal behaviour of polypropylene fractions: 2. The multiple melting peaks, Polymer. 34 (1993) 4083–4088. https://doi.org/10.1016/0032-3861(93)90670-6.
[58] J. Gasia, L. Miró, A. de Gracia, C. Barreneche, L. Cabeza, Experimental Evaluation of a Paraffin as Phase Change Material for Thermal Energy Storage in Laboratory Equipment and in a Shell-and-Tube Heat Exchanger, Applied Sciences. 6 (2016) 112. https://doi.org/10.3390/app6040112.
[59] Y. Kou, S. Wang, J. Luo, K. Sun, J. Zhang, Z. Tan, Q. Shi, Thermal analysis and heat capacity study of polyethylene glycol (PEG) phase change materials for thermal energy storage applications, The Journal of Chemical Thermodynamics. 128 (2019) 259–274. https://doi.org/10.1016/j.jct.2018.08.031.
[60] H. Zhu, Y. Lv, T. Duan, M. Zhu, Y. Li, W. Miao, Z. Wang, In-situ investigation of multiple endothermic peaks in isomorphous poly(3-hydroxybutyrate-co-3-hydroxyvalerate) with low HV content by synchrotron radiation, Polymer. 169 (2019) 1–10. https://doi.org/10.1016/j.polymer.2019.01.077.
[61] M. Qian, P. Cao, M.A. Easton, S.D. McDonald, D.H. StJohn, An analytical model for constitutional supercooling-driven grain formation and grain size prediction, Acta Materialia. 58 (2010) 3262–3270. https://doi.org/10.1016/j.actamat.2010.01.052.
[62] M.E. Glicksman, Principles of Solidification: An Introduction to Modern Casting and Crystal Growth Concepts, Materials Today. 14 (2011) 502. https://doi.org/10.1016/S1369-7021(11)70218-8.
[63] A.M. Reyna, Modélisation du stockage de chaleur par changement de phase d'alliages à composition binaire soumis à un refroidissement contrôlé, (n.d.) 265.
[64] M. Duquesne, A. Godin, E.P. del Barrio, F. Achchaq, Crystal growth kinetics of sugar alcohols as phase change materials for thermal energy storage, Energy Procedia. 139 (2017) 315–321. https://doi.org/10.1016/j.egypro.2017.11.214.
[65] M.A. Jaafar, D.R. Rousse, S. Gibout, J.-P. Bédécarrats, A review of dendritic growth during solidification: Mathematical modeling and numerical simulations, Renewable and Sustainable Energy Reviews. 74 (2017) 1064–1079. https://doi.org/10.1016/j.rser.2017.02.050.
[66] Z. Younsi, L. Zalewski, S. Lassue, D.R. Rousse, A. Joulin, A Novel Technique for Experimental Thermophysical Characterization of Phase-Change Materials, International Journal of Thermophysics. 32 (2011) 674–692. https://doi.org/10.1007/s10765-010-0900-z.
[67] A. Joulin, Z. Younsi, L. Zalewski, S. Lassue, D.R. Rousse, J.-P. Cavrot, Experimental and numerical investigation of a phase change material: Thermal-energy storage and release, Applied Energy. 88 (2011) 2454–2462. https://doi.org/10.1016/j.apenergy.2011.01.036.

[68] A. Joulin, L. Zalewski, S. Lassue, H. Naji, Experimental investigation of thermal characteristics of a mortar with or without a micro-encapsulated phase change material, Applied Thermal Engineering. 66 (2014) 171–180. https://doi.org/10.1016/j.applthermaleng.2014.01.027.

[69] P. Tittelein, S. Gibout, E. Franquet, K. Johannes, L. Zalewski, F. Kuznik, J.-P. Dumas, S. Lassue, J.-P. Bédécarrats, D. David, Simulation of the thermal and energy behaviour of a composite material containing encapsulated-PCM: Influence of the thermodynamical modelling, Applied Energy. 140 (2015) 269–274. https://doi.org/10.1016/j.apenergy.2014.11.055.

[70] D. Mazzeo, Thermal field and heat storage in a cyclic phase change process caused by several moving melting and solidification interfaces in the layer, International Journal of Thermal Sciences. (2018) 27.

[71] D. Mazzeo, G. Oliveti, A. de Gracia, J. Coma, A. Solé, L.F. Cabeza, Experimental validation of the exact analytical solution to the steady periodic heat transfer problem in a PCM layer, Energy. 140 (2017) 1131–1147. https://doi.org/10.1016/j.energy.2017.08.045.

[72] B. Tang, C. Wu, M. Qiu, X. Zhang, S. Zhang, PEG/SiO2–Al2O3 hybrid form-stable phase change materials with enhanced thermal conductivity, Materials Chemistry and Physics. 144 (2014) 162–167. https://doi.org/10.1016/j.matchemphys.2013.12.036.